Economic Geology, v. 101, pp. 33–57

Regional Surficial Geochemistry of the Northern Great Basin

Steve Ludington,†

U.S. Geological Survey, 345 Middlefield Road, Mail Stop 901, Menlo Park, California 94025

Helen Folger,

U.S. Geological Survey, 954 National Center, Reston, Virginia 20192

Boris Kotlyar,

3653 Longdon Commons, Fremont, California 94538

Victor G. Mossotti,

U.S. Geological Survey, 345 Middlefield Road, Mail Stop 901, Menlo Park, California 94025

Mary Jane Coombs,

6503 Madrid Road, Goleta, California 93117

and Thomas G. Hildenbrand

U.S. Geological Survey, 345 Middlefield Road, Mail Stop 901, Menlo Park, California 94025

Abstract

The regional distribution of arsenic and 20 other elements in stream-sediment samples in northern Nevada and southeastern Oregon was studied in order to gain new insights about the geologic framework and patterns of hydrothermal mineralization in the area. Data were used from 10,261 samples that were originally collected during the National Uranium Resource Evaluation (NURE) Hydrogeochemical and Stream Sediment Reconnaissance (HSSR) program in the 1970s. The data are available as U.S. Geological Survey Open-File Report 02-0227.

The data were analyzed using traditional dot maps and interpolation between data points to construct high-resolution raster images, which were correlated with geographic and geologic information using a geographic information system (GIS). Wavelength filters were also used to deconvolute the geochemical images into various textural components, in order to study features with dimensions of a few kilometers to dimensions of hundreds of kilometers.

The distribution of arsenic, antimony, gold, and silver is different from distributions of the other elements in that they show a distinctive high background in the southeast part of the area, generally in areas underlain by the pre-Mesozoic craton. Arsenic is an extremely mobile element and can be used to delineate structures that served as conduits for the circulation of metal-bearing fluids. It was used to delineate large crustal structures and is particularly good for delineation of the Battle Mountain-Eureka mineral trend and the Steens lineament, which corresponds to a post-Miocene fault zone. Arsenic distribution patterns also delineated the Black Rock structural boundary, northwest of which the basement apparently consists entirely of Miocene and younger crust.

Arsenic is also useful to locate district-sized hydrothermal systems and clusters of systems. Most important types of hydrothermal mineral deposit in the northern Great Basin appear to be strongly associated with arsenic; this is less so for low-sulfidation epithermal deposits.

In addition to individual elements, the distribution of factor scores that resulted from principal component studies of the data was used. The strongest factor is characterized by Fe, Ti, V, Cu, Ni, and Zn and is used to map the distribution of distinctive basalts that are high in Cu, Ni, and Zn and that appear to be related to the Steens Basalt. The other important factor is related to hydrothermal precious metal mineralization and is characterized by Sb, Ag, As, Pb, Au, and Zn. The map of the distribution of this factor is similar in appearance to the one for arsenic, and we used wavelength filters to remove regional variations in the background for this factor score. The resulting residual map shows a very strong association with the most significant precious metal deposits and districts in the region. This residual map also shows a number of areas that are not associated with known mineral deposits, illustrating the utility of the method as a regional exploration tool. A number of these prospective areas are distant from known significant mineral deposits.

The deconvolution of the spatial wavelength structure of geochemical maps, combined with the use of large regional geochemical data sets and GIS, permits new possibilities for the use of stream-sediment geochemistry in the study of large-scale crustal features as well as the isolation of mineral-district scale anomalies.

† Corresponding author: e-mail, slud@usgs.gov

0361-0128/06/3566/33-25 $6.00

Introduction

THIS STUDY provides new insights into the geologic framework and patterns of hydrothermal mineralization in the northern Great Basin of the United States, based on a very large data set of stream-sediment and soil analyses. The data used include new analyses of 21 elements in more than 10,000 samples that were originally collected during the National Uranium Resource Evaluation (NURE) program in the 1970s. The locations of the samples and the study area are shown in Figure 1, and an index map showing place names mentioned in this report is shown in Figure 2. The samples were analyzed over a decade, beginning in 1992, and the data, along with some simple maps, are available as U.S. Geological Survey Open-File Report 02-0227 (Coombs et al., 2002). That report also contains detailed technical information about sample media type and size fraction, about the history of these data, and about their precision, accuracy, and quality control.

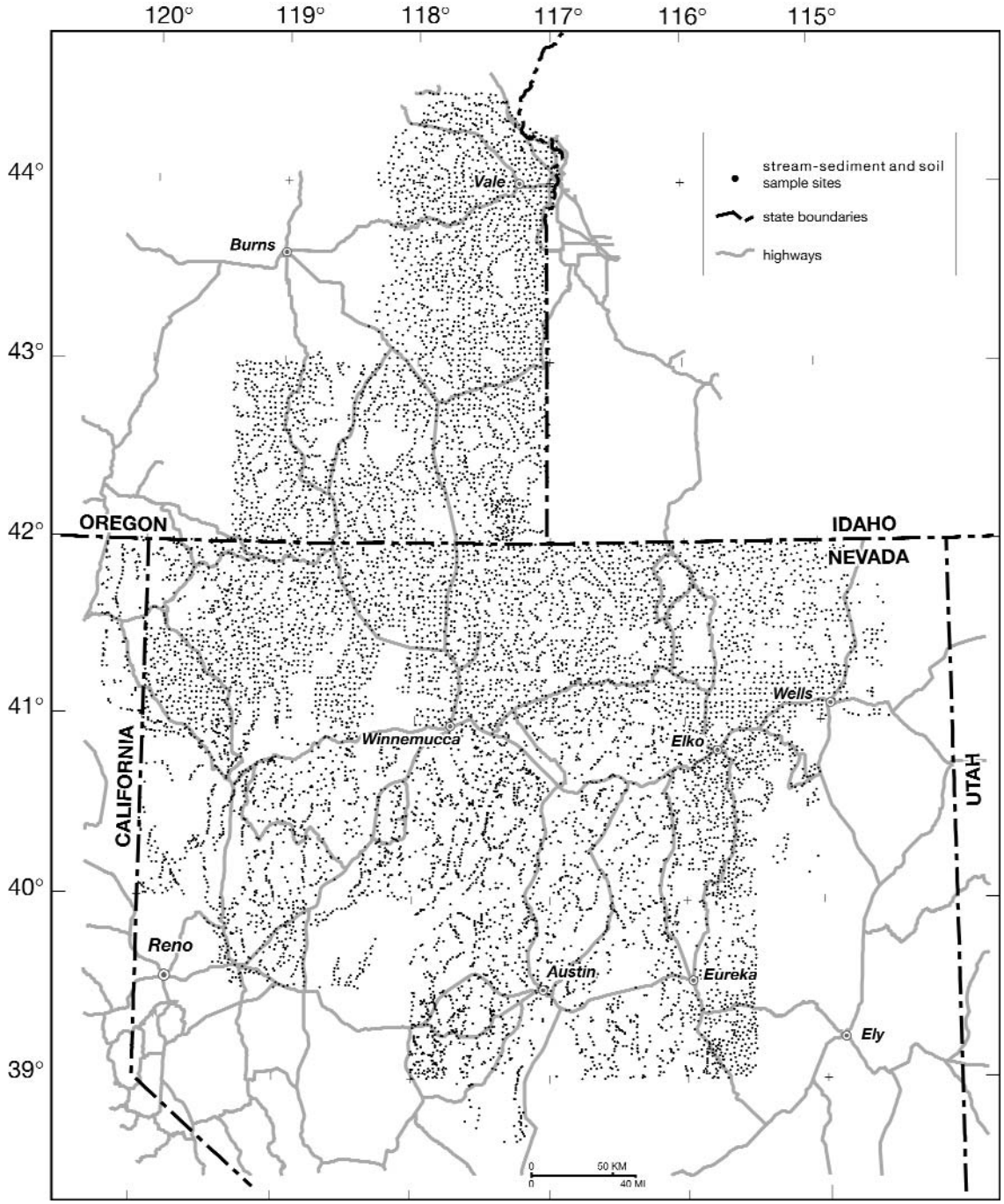

FIG. 1. Location map showing the area studied and the sample sites. The data are reported in Coombs et al. (2002).

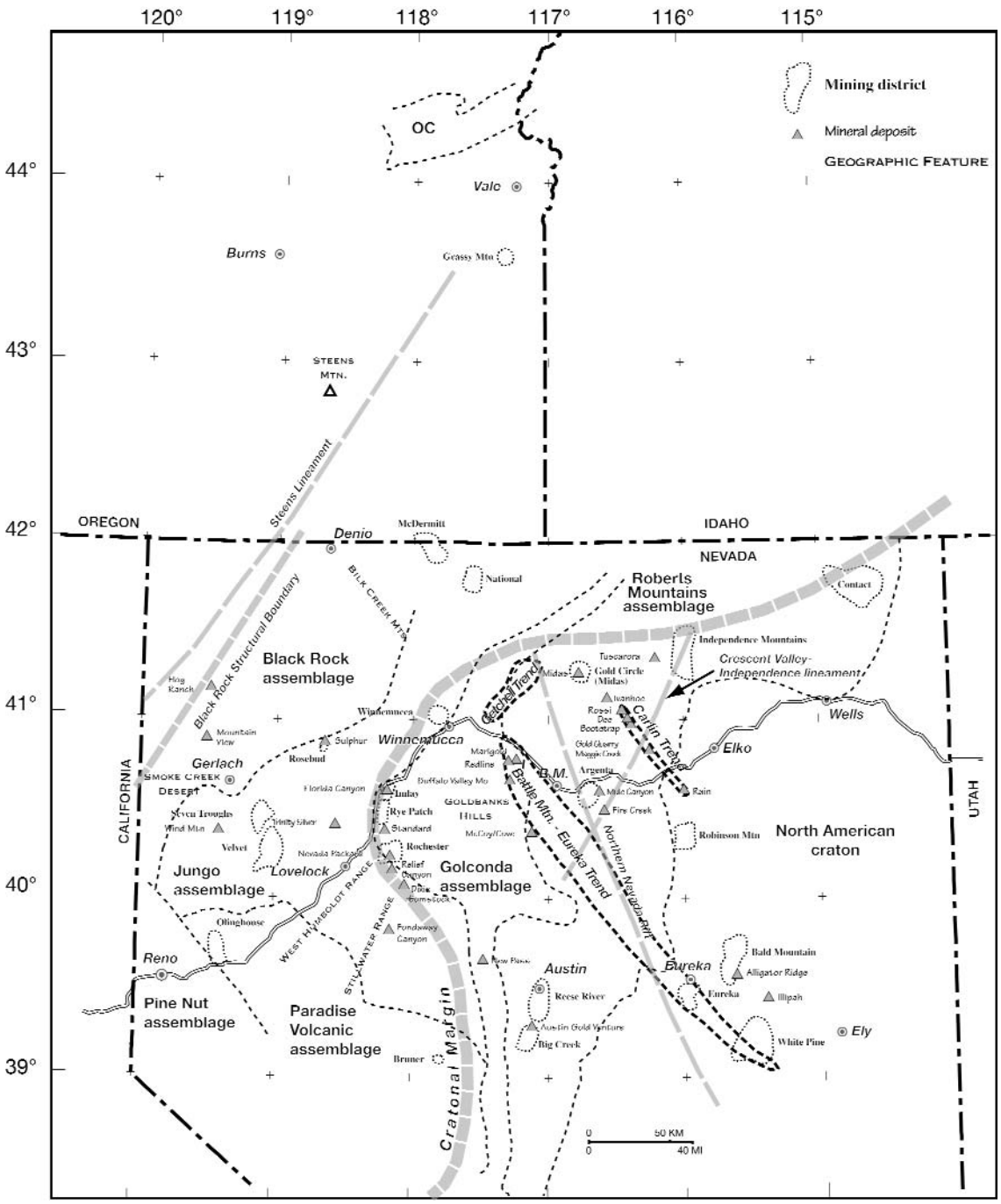

FIG. 2. Index map of the study area, showing place names mentioned in the text. Lithologic assemblages are from Ludington et al. (1996b), except OC, which refers to all crustal rocks in eastern Oregon (Miller et al., 2003).

These new analyses provide a unique opportunity to test the application of high-quality, closely spaced, stream-sediment and soil geochemical data to a large, geologically complex region. These samples were collected at a spacing that makes them ideal for the identification of district-sized geochemical anomalies at map scales between 1:250,000 and 1:5,000,000. Because most of the samples were collected in the 1970s, before most large-scale industrial gold mining in northern Nevada, the data provide a unique look at premining baseline data on the distribution of metals at the surface in the northern part of the Great Basin. The data include analyses for many environmentally important elements, including arsenic, antimony, and base metals, providing important information on the natural distribution of these elements. In addition, resampling of NURE sites could now provide an important measure of the temporal changes that may or may not have accompanied subsequent metal development and production. The data also contribute new insight to our understanding of

average crustal compositions, as they permit the characterization of discrete geochemical provinces, with dimensions ranging from tens to hundreds of kilometers, as well as the identification of crustal boundaries and large structures that extend for hundreds of kilometers. They also permit an evaluation of the common, but questionable, practice of extrapolation of the geochemical baselines of small areas to large regions underlain by the same geologic map unit.

Previous Studies

Regional studies

Only two geochemical studies that included the entire northern Great Basin at the scale and scope of this study have been published previously: the aerial gamma-ray spectrometric study of K, Th, and U by Duval (1991) and Duval and Riggle (1999), and the nationwide soil study of Shacklette and Boerngen (1984), which was given a modern presentation by Gustavsson et al. (2001). The gamma-ray spectrometry maps mirror the general distribution of silicic (K- and U-rich) volcanic rocks throughout northern Nevada and southeastern Oregon. The maps of Shacklette and Boerngen (1984) include only 23 samples within the present study area (Fig. 1), primarily along a transect that follows a major highway across northern Nevada.

A newer study by Rice (1999) provides analyses of nine elements (As, Cd, Cr, Cu, Hg, Ni, Pb, Se, and Zn) in 541 stream bed-sediment samples from 20 study areas across the conterminous United States. These data were collected during the 1990s and provide a nationwide comparison for the data from the northern Great Basin. Table 1 shows the median values of the seven elements that the data of Rice (1999) and our northern Great Basin data have in common.

The northern Great Basin average values are lower than the nationwide averages for all seven elements. Perhaps the best explanation, and one proposed by Rice (1999), is that the nationwide data set contains a substantial number of samples affected by industrial and urban runoff, but a large part of the difference may also be due to the distinctly smaller size fraction used by Rice (1999) or to differences in completeness of digestion (especially Cr). The lead values in the Great Basin might be expected to be low, because much of the study area is west of the ancient continental margin and lacks substantial radiogenic lead. In addition, the sparse population may mean that there is minimal anthropogenic lead in the Great Basin data.

Mihalasky (2001) used original NURE data in a study designed to delineate areas likely to contain undiscovered precious metal deposits in north-central Nevada.

Studies within the Great Basin

Several geochemical studies in the Great Basin were carried out during the U.S. Geological Survey's Conterminous United States Mineral Assessment Program (CUSMAP). Nash (1987) and Nash and Siems (1988) published an interpretation of samples from the Tonopah 1° × 2° Quadrangle at the southern margin of the study area based on semiquantitative spectrographic analysis of newly collected samples from 1,217 sites. Kilburn et al. (1990) studied the Reno 1° × 2° Quadrangle, in the southwest part of the study area, using reanalysis of existing NURE Hydrogeochemical and Stream Sediment Reconnaissance (HSSR) samples for a limited suite of elements and made a brief interpretation to support the mineral resource assessment in John et al. (1993). Chaffee (1988) published a geochemical study of the Walker Lake 1° × 2° Quadrangle, which adjoins our study area on the southwest, that was based on semiquantitative spectrographic analysis of nonmagnetic heavy mineral concentrates. All of these studies used different analytical methods or measured a different group of elements, and we did not attempt to directly compare their data with the northern Great Basin data presented here.

In addition, earlier studies by one of the present authors (Kotlyar et al., 1998) were an impetus for the present study. Kotlyar used the upward continuation algorithm that is commonly used to manipulate geophysical data, with geochemical data, in order to suppress short-wavelength features. This work stimulated the research that led to our use of symmetric band-pass wavelength filters (Fourier-transform analysis) to decompose the geochemical maps into distinct wavelength intervals as described below.

TABLE 1. Median Values of Concentrations of Seven Selected Elements (in parts per million) of Stream-Sediment Samples from Northern Great Basin and Nationwide

Area	As	Cd	Cr	Cu	Pb	Ni	Zn
Northern Great Basin	4.5	0.25	62	19.6	10.7	20	58
Nationwide (Rice, 1999)	6.3	0.4	64	27	27	27	110

Data Sources

The experience of Kotlyar et al. (1998) in attempting to use original NURE HSSR data for arsenic generated concerns about the quality and usefulness of the original data. As documented by Coombs et al. (2002), the original data for this study area were obtained by the NURE program, using a wide variety of analytical methods on potentially disparate sample media, and results for individual elements are commonly not comparable from quadrangle to quadrangle. As an example, Figure 3 shows a map of arsenic distribution in the study area, based on the original NURE HSSR analyses. Although some of the features of our newer maps are represented here, arsenic concentrations for the McDermitt and Elko quadrangles are clearly lower than that for the adjacent Winnemucca, Lovelock, and Millett quadrangles. Arsenic in the McDermitt and Elko quadrangles was a supplemental analysis by the Savannah River Laboratory, and the analytical method is unknown. The other quadrangles were analyzed by the Lawrence Livermore Laboratory, and most elements (including arsenic) were analyzed by neutron activation. In addition, NURE HSSR samples from many of the quadrangles were never analyzed for arsenic. Thus, there are some significant analytical problems between quadrangles, and regional interpretations using the original data appear problematic.

The newer methods (Coombs et al., 2002) used to provide the data in our study are both more precise and more accurate than the first-generation NURE values. Analyses for this study are by inductively coupled plasma-atomic emission spectroscopy (ICPMS) after dissolution by acid and also by an organic extraction. This protocol also corresponds closely to the analytical suite being used for the National Geochemical

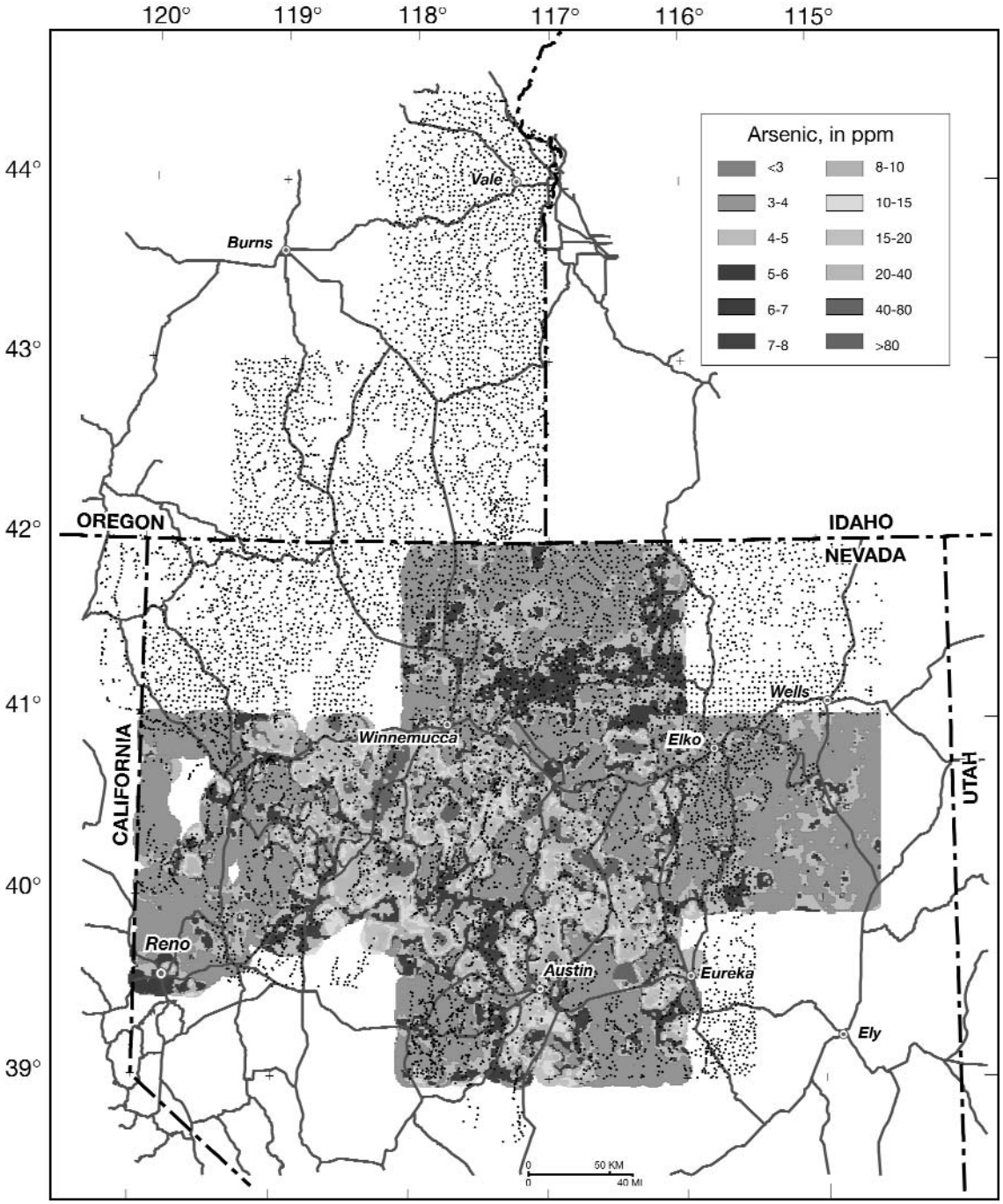

FIG. 3. Map showing distribution of arsenic, based on original NURE data. Data were taken from Smith (2001) and interpolated to a 2-km grid using inverse distance weighting methods. Contour intervals are the same as those used for arsenic in Coombs et al. (2002) and in Figures 9 and 11. Note that the data for the Elko 1° × 2° quadrangle (easternmost) and the McDermitt quadrangle (northernmost) never exceed 15 ppm, whereas large areas of the other three quadrangles do.

Survey (Grosz and Grossman, 2000; U.S. Geological Survey, 2004).

In 1992, the U.S. Geological Survey, in conjunction with the U.S. Bureau of Land Management and the U.S. Bureau of Mines, undertook a mineral-resource assessment of the Winnemucca-Surprise resource assessment area, which was composed of the Bureau of Land Management's Winnemucca district in northwest Nevada and the Susanville district in northeast California and northwest Nevada. In the course of this study, 3,551 previously collected NURE HSSR stream-sediment and soil samples were reanalyzed in U.S. Geological Survey laboratories. In addition, in order to assure complete sampling coverage for the mineral-resource assessment, the U.S. Geological Survey analyzed 321 newly collected stream-sediment samples. The data, along with sampling and analysis protocols, and some information on quality

control, were reported in King et al. (1996), and a preliminary interpretation was also published (King et al., 1996; Peters et al., 1996).

Also beginning in 1992, the U.S. Geological Survey performed a mineral-resource assessment of the Malheur, Jordan, and Andrews Bureau of Land Management resource areas in Oregon and Idaho. During this assessment, 2,516 previously collected NURE HSSR stream-sediment and soil samples were reanalyzed in USGS laboratories. In addition, the U.S. Geological Survey collected and analyzed 161 new stream-sediment samples. These data were stored in the USGS geochemical database; parts of this database, including the Malheur-Jordan-Andrews data, can be found in Baedecker et al. (1998).

The U.S. Geological Survey, in collaboration with the Bureau of Land Management, began a mineral-resource assessment of the Humboldt River basin in northern Nevada in October 1995 (Wallace et al., 2004). In support of this assessment, 3,712 previously collected NURE HSSR stream-sediment and soil samples from the McDermitt, Wells, Winnemucca, Elko, Millett, Ely, and Tonopah 1° × 2° quadrangles were reanalyzed by the Nevada Bureau of Mines and Geology, under contract to the U.S. Geological Survey, using the same analytical protocols. These data are available on a CD-ROM (Folger, 2000).

Figure 4 shows the location of the studies described above. Further details can be found in Coombs et al. (2002).

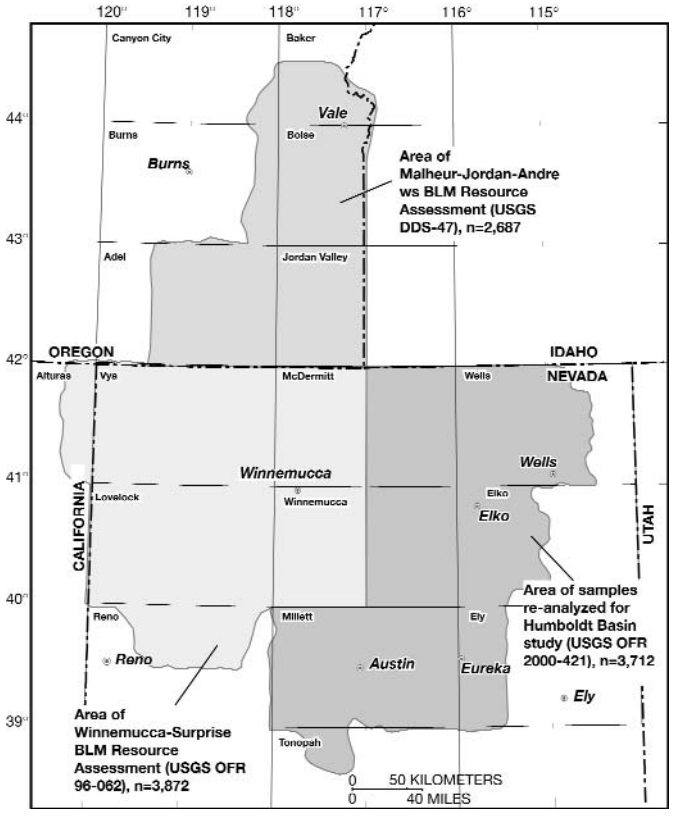

FIG. 4. Map showing sources of data used in this study and 1° × 2° quadrangle names (modified from Coombs et al., 2002).

Data Quality

Analyzing data quality is complex and involves evaluation of the sample collection and sample preparation techniques, as well as the more familiar concerns about inter- and intralaboratory variability. Many of these concerns are discussed in some detail in Coombs et al. (2002). Of primary concern is that many of the samples in our study area, primarily in the Elko, McDermitt, and Wells quadrangles, were termed soil samples under the NURE program, and apparently were not collected from active or dry streambeds (Fig. 5). We examined the data to see if the sample medium was related to composition and concluded that there is reasonable continuity across the quadrangle boundaries in question, and that there is no reason to avoid mixing results from the soil samples with results from stream-sediment samples (Coombs et al., 2002). Figure 6 shows one east-west profile across the study area that demonstrates this continuity.

Thirty-five elements are common to all three data sets in the previous studies, including 10 (Ag, As, Au, Bi, Cd, Cu, Ga, Mo, Pb, and Zn) for which data were obtained by at least two different analytical methods. Because we were more interested in spatial distribution patterns than absolute values, we used spatial discontinuities between data sets in the smoothed element maps to disqualify an element from further interpretation. Other reasons for eliminating some elements included contamination during sample preparation, very different detection limits among the three source data sets, and elements that exhibited only a very small range of values. The quality evaluation process led us to focus on 21 elements (Ag, As, Au, Ba, Ca, Ce, Cu, Fe, K, La, Mg, Na, Ni, Pb, Sb, Sr, Th, Ti, V, Y, and Zn) in the present study.

Partial versus total analyses

The samples from our study area were analyzed for several elements by two different methods. The first method is considered a total analysis and involves dissolving an aliquot of the sample in a series of acid digestions, including hydrofluoric acid, and analysis by inductively coupled plasma-atomic emission spectrometry (ICP-AES; Briggs, 1996). This method normally dissolves almost all the material in the sample, thus it is termed a total analysis; it is capable of analyzing 40 elements simultaneously at detection limits useful for most environmental and mineral exploration studies. A second method involves the partial digestion of a second aliquot of the sample using concentrated hydrochloric acid and hydrogen peroxide, followed by extraction into an organic solvent, and allows lower detection limits and better precision at low concentrations (Motooka, 1996). This second method dissolves metals bound loosely to iron oxide and clay minerals, and some sulfide minerals, but does not dissolve silicate minerals; thus it is termed a partial analysis.

Figure 7 shows the values for partial versus total analyses for As, Pb, Ag, Cd, Cu, and Zn. On these log-log diagrams, if all the metal in the sample is loosely bound or resides in easily soluble minerals, the points would show a 1:1 correlation (solid diagonal lines, Fig. 7). For all the metals shown, this behavior is most common at higher overall concentrations. If, on the other hand, most of the metal in a sample is tightly bound in silicate minerals, the points will fall below the 1:1

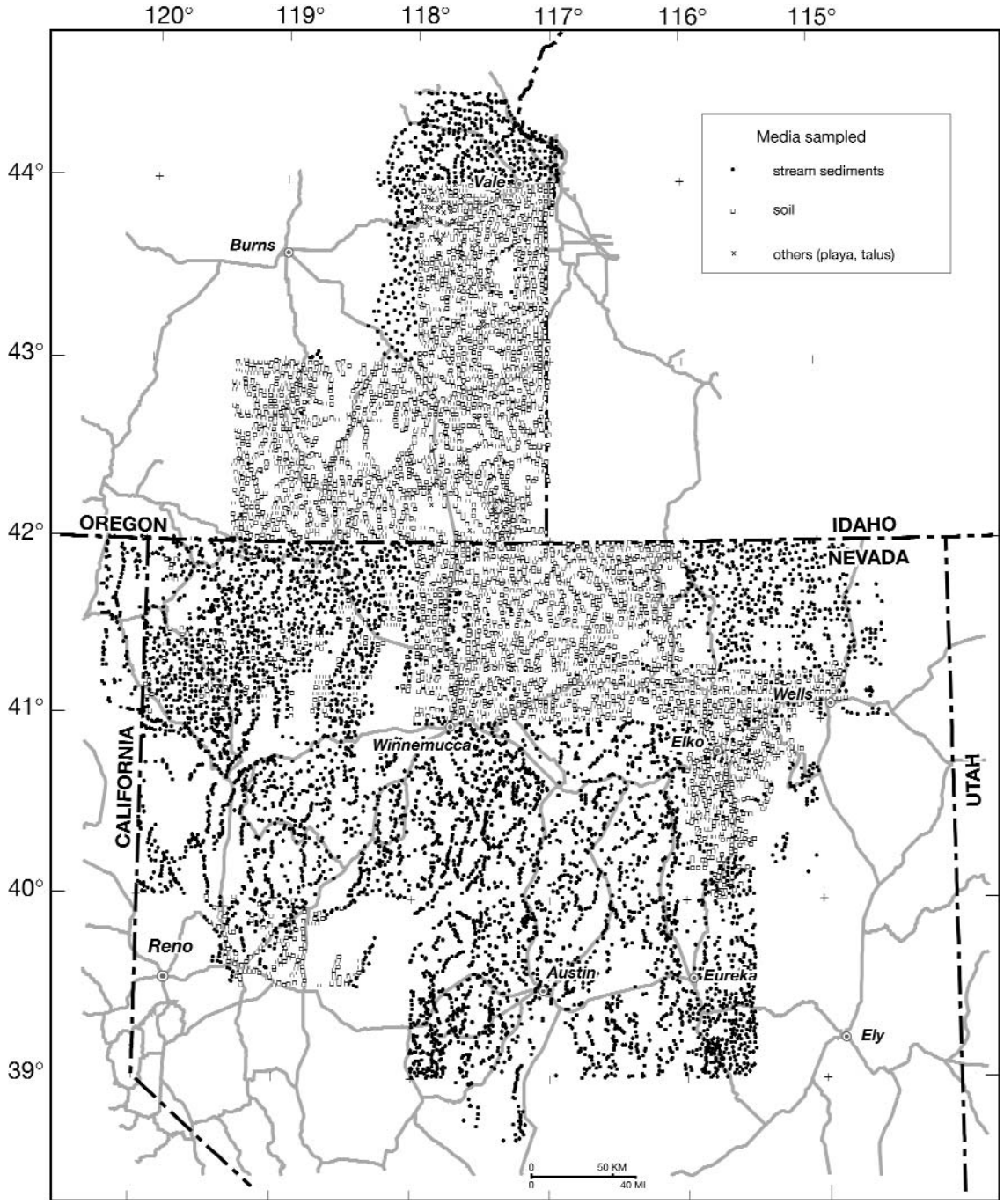

FIG. 5. Map showing the distribution of samples classified as stream sediments and as soils in the study area. NURE sample types 59 and 62 (Smith, 2001) are considered soil samples; other sample types are stream sediments (see Coombs et al., 2002, for detailed discussion).

correspondence line, near the horizontal axis. The dashed lines on the plots in Figure 7, which represent a ratio of 1.5 total/1 partial, nominally divide the samples into two groups: one above the line, in which a significant proportion of the metal resides primarily in a readily soluble state (in Mn-Fe oxide, sulfate, chloride, carbonate or sulfide minerals, or adsorbed on iron oxide or clay minerals), and a second, below the line, in which the metal resides primarily in a less soluble state (in silicate minerals).

A confounding issue, most prominent on the plots for arsenic and lead, is related to analytical uncertainty. On a log-log plot, a constant uncertainty of a few parts per million (ppm) displays as a fan about the line representing correspondence, widening at lower concentrations; thus, at low concentrations near the detection limit, some of the points below the dashed lines are due to analytical uncertainty. Nevertheless, all the plots except copper (and possibly zinc) show a marked asymmetry toward low partial determinations,

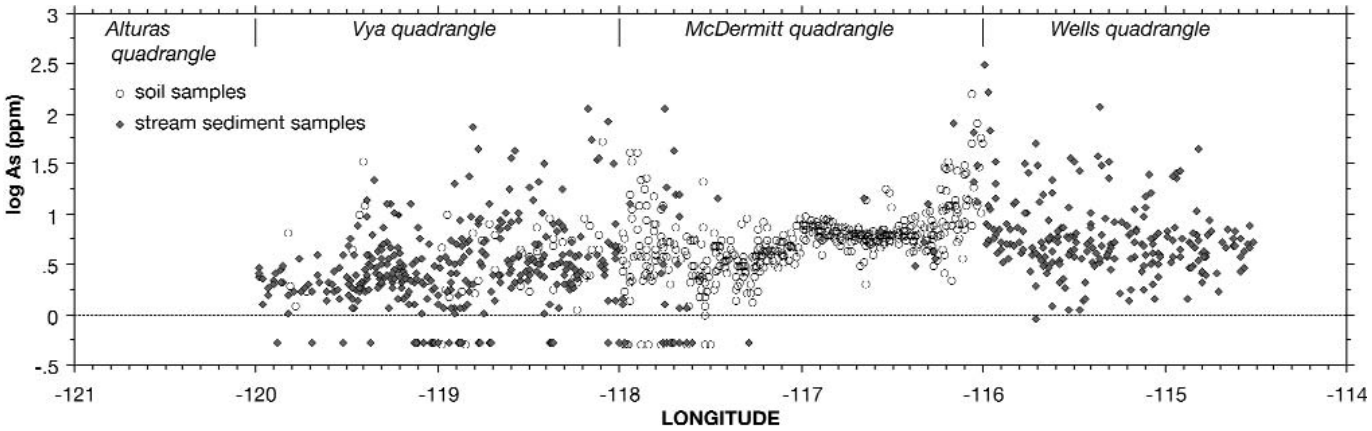

FIG. 6. East-west profile of arsenic values at latitude 41.6° ± 0.2° N latitude. Although there appears to be a somewhat greater amount of variability in the values for stream-sediment samples than for soil samples, the data are spatially continuous.

suggesting that a significant proportion of these metals is found in a less soluble state.

Lead appears soluble in 62 percent of the samples, suggesting that it resides in silicates like feldspar. Zinc, cadmium, and silver all display similar proportions, with about one third occurring in insoluble components.

Arsenic and copper behave differently. In the great majority (77% for arsenic and 84% for copper) of the samples, these elements reside in a loosely bound state, likely adsorbed on iron oxide and clay minerals, as well as in sulfides. In addition, when plotted in a map, most samples with insoluble arsenic lie in the northern part of the study area, in areas underlain by Miocene basalt, where the arsenic likely resides in silicate minerals in unweathered basalt.

Arsenic is known to be mobile in the surficial environment, and Theodore et al. (2003) have shown directly, using X-ray absorption fine structure spectroscopy, that arsenic is commonly fixed in stream sediments as an element adsorbed onto clay minerals. Their conclusions regarding arsenic mobility and fixation are supported by our very large data set.

At the higher values that would be most likely due to hydrothermal sulfide mineralization, all the metals show compelling correspondence between the two analytical methods (total and partial), which supports the credibility of the determinations. The higher values also correspond well with the original NURE HSSR neutron activation analyses for arsenic in the Winnemucca, Lovelock, and Millett quadrangles reported by Los Alamos National Laboratories (Smith, 2001). In the discussion and analysis that follows, we have used the partial analyses for Ag, As, Cd, Cu, Pb, Sb, and Zn, because of the high sensitivity and to reduce the amount of qualified data.

Methods of Interpretation

Because of the size and geologic diversity of the study area, the spatial variations in the data are more important than statistics of an element's population for the entire data set. Most of the elements in our data set should not be expected to represent a single population and probably do not. A variety of methods are available to help derive meaningful conclusions from a large amount of data, but the availability of modern Geographic Information System (GIS) software has made the present study feasible.

Point-symbol maps

Highlighting the highest and lowest quartiles of the data demonstrates prominent spatial patterns in the data. The elements fall into three general groups. The patterns shown by As, Sb, Ag, Au, and, to a lesser extent, Pb and Zn, clearly define some important mineral deposit trends and groupings and are generally higher in the southeast half of the study area (Fig. 8A). Cu, Ti, V, Sc, Ni, Co, and, to a lesser extent, Fe show a cluster of high values in southeast Oregon and are generally higher in the northwest half of the study area (Fig 8B). The rest of the elements do not display simply discernible patterns on the point-symbol maps. This preliminary evaluation suggested that the elements commonly found in sulfide-bearing mineral deposits are spatially distributed very differently than those found in silicate and oxide minerals in common rocks and that they yield different information about geology. These observations are further refined using principal component analysis (see below).

Gridding methods

When sample coverage is dense, the display of geochemical data can be enhanced by the use of pixel-based raster images based on interpolation between data points. Although interpolation may sometimes distort the spatial variability, the method is effective in providing an integrated view of spatial variability at various scales. Our grids were generated using inverse distance weighting, calculating the value at each grid point as the average of all data points within 10 km of the grid point, weighted by the inverse square of their distance from the grid point. Grids were generated using both 1- and 2-km cells. The 10-km averaging radius results in the blank areas within the maps (Fig. 9), which are areas that are more than 10-km distant from any sample point. The grids are least reliable near these blank areas and at the margins of the maps. Most areas of the maps, however, have sample points within 2 to 3 km. Care should be exercised in interpretation near the map edges, as the interpolation methods are not well constrained there. Similar care should be applied to very small

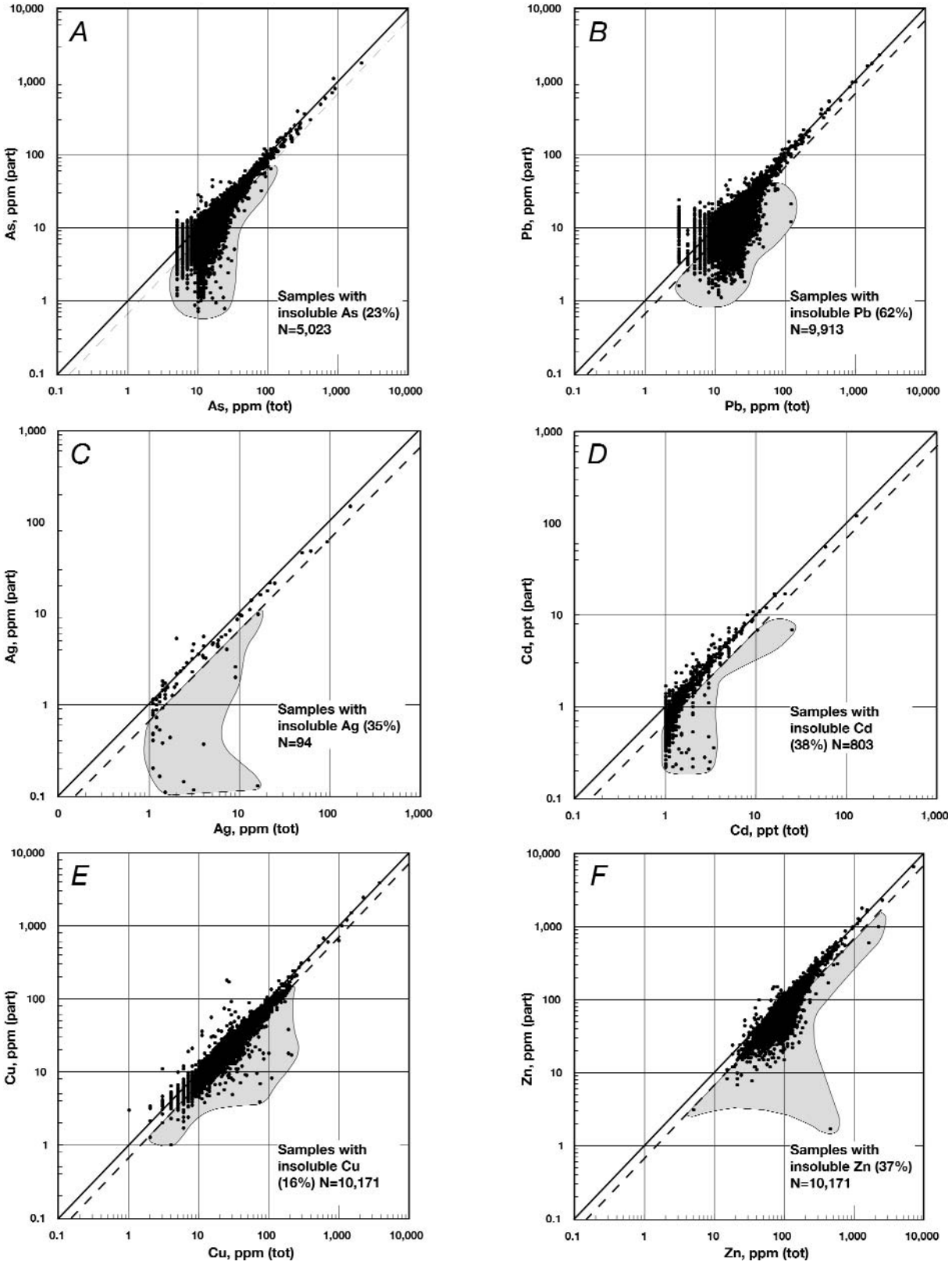

FIG. 7. Plots showing comparison of partial vs. total digestion methods for (A) arsenic, (B) lead, (C) silver, (D) cadmium, (E) copper, and (F) zinc. Only points for which both methods yielded a valid determination (above the detection limit) are plotted; the number of points plotted is indicated by N. Shaded areas highlight samples with primarily insoluble metal and the proportion is indicated. Solid diagonal line represents 1/1 correspondence; dashed diagonal line represents the ratio total/partial of 1.5/1. See text for further discussion.

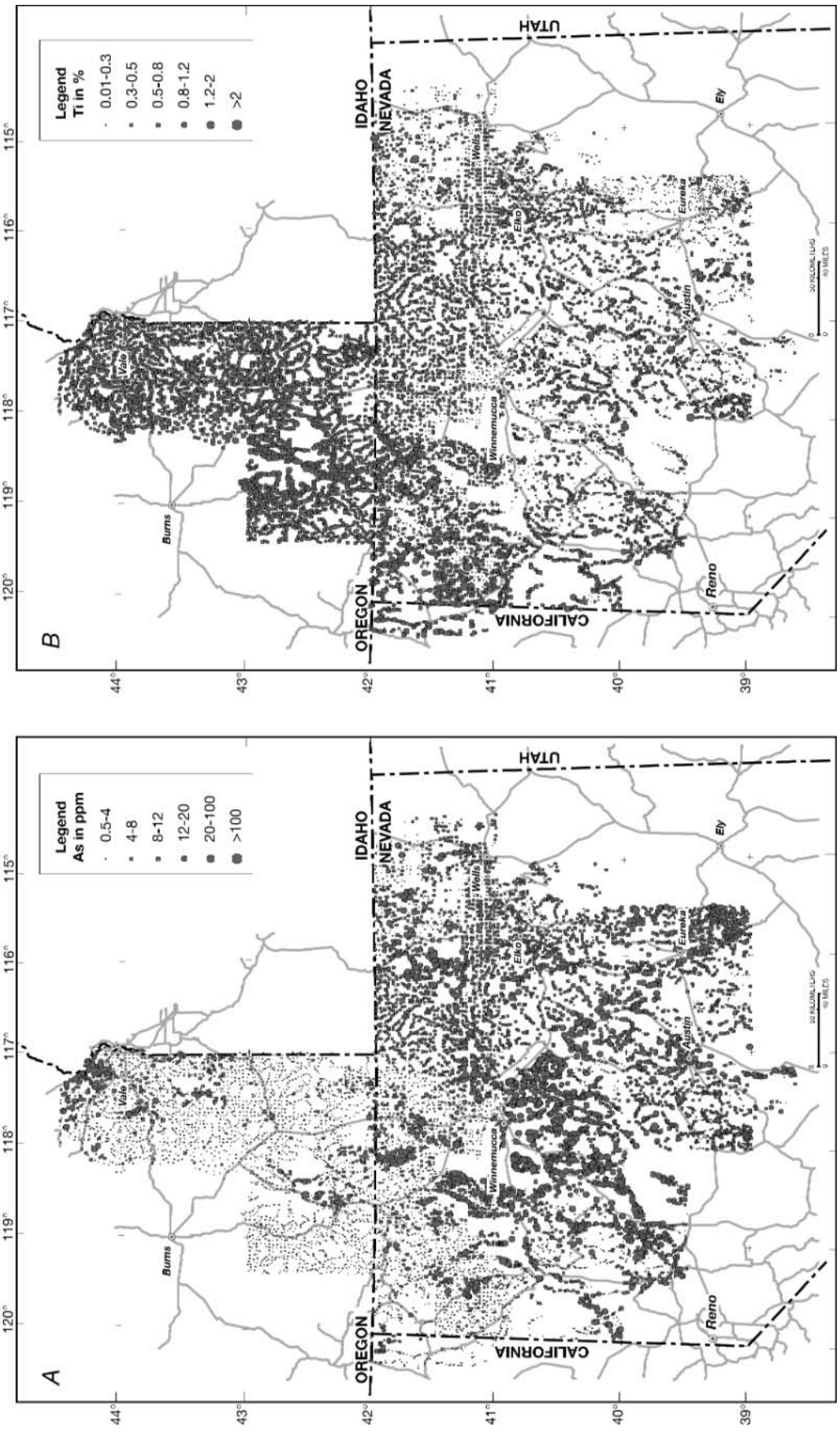

FIG. 8. Point-symbol maps (Howarth, 1983) comparing data for (A) arsenic and (B) titanium.

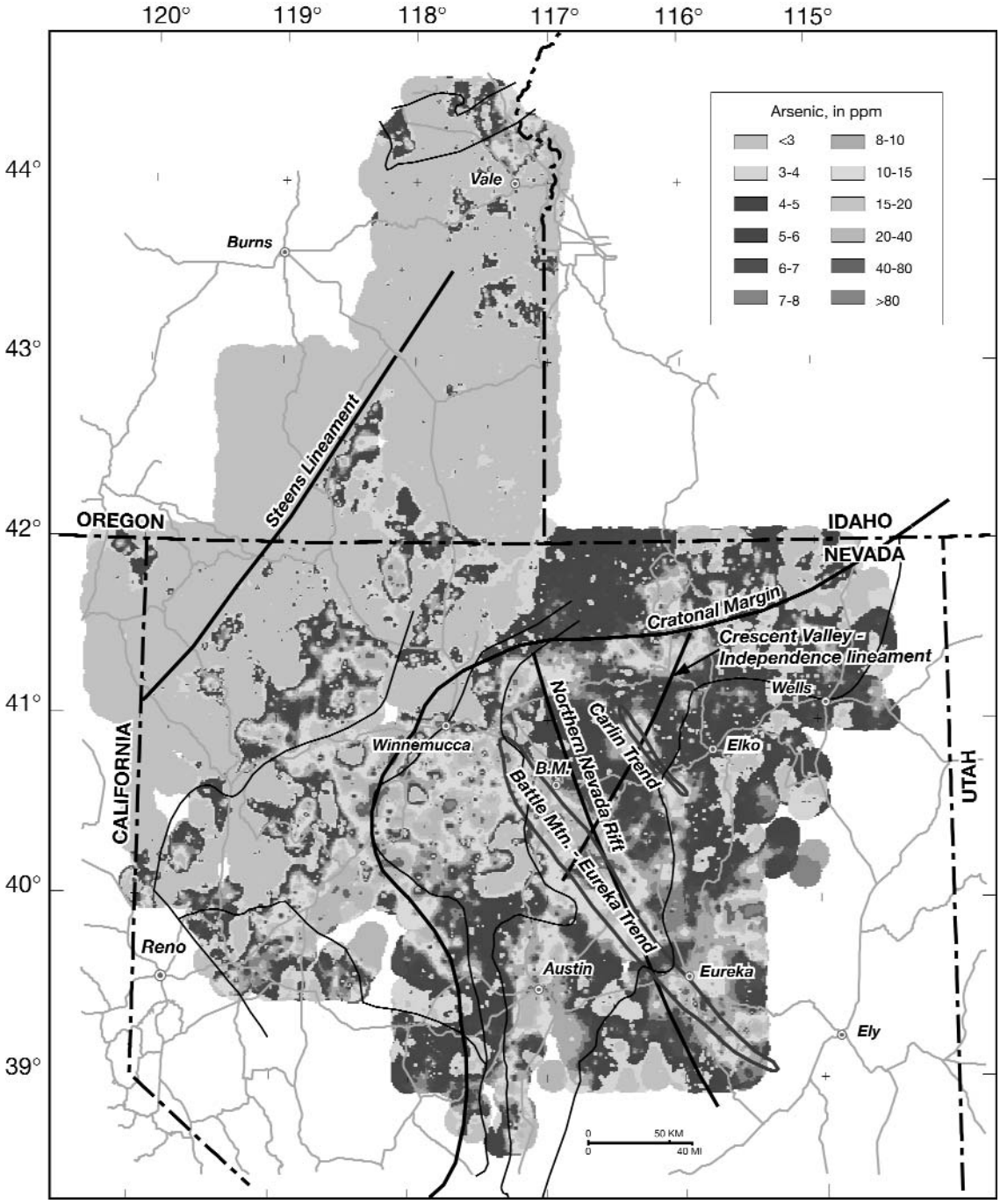

FIG. 9. Map showing arsenic distribution before filtering into spatial wavelength intervals. Light black lines showing assemblage boundaries are identified in Figure 2. B.M. = town of Battle Mountain.

anomalies that may be an artifact of the gridding process if they do not contain an actual sample point. Figure 9 shows the gridded map for arsenic.

Smoothing methods

The elemental grids that we generated (see Coombs et al., 2002) demonstrate that, for some elements, particularly arsenic and antimony, there are important regional differences in the geochemical baseline on a scale of hundreds of kilometers. Superimposed on this large-scale variability are smaller features like mineral deposit trends, clusters, and districts with dimensions of tens of kilometers, as well as features that probably represent individual hydrothermal systems, with dimensions of a few kilometers.

Spatial geochemical variability can be present at a wide variety of scales, and regions with similar characteristics can have dimensions that range from the scale of individual mineral grains to features that are hundreds of kilometers in

extent. We used spatial wavelength filters to separate the signal components for features of various sizes. The minimum size for a discernable feature in our study is about 2 to 3 km, the same as the sample spacing. This spatial variability can be viewed as having wave properties, such that small-scale local variability is a short-wavelength (high frequency) signal, and large-scale regional variability is a long-wavelength (low frequency) signal. In a manner entirely analogous to the electronic filtering of sound to increase clarity, wavelength filters can be used to analyze the variability and to isolate the different types of signals.

In order to decompose these maps into various textural components, we computed the spatial frequency structure of the grid surfaces and derived a series of band-pass wavelength filters to separate the signal into distinct wavelength intervals, each with varying degrees of smoothness (Phillips, 2001).

Figure 10 shows the filters that we used to decompose the arsenic map. The regional filter passes low frequencies that generate a very smooth map (Fig. 11A). The noise filter passes short-wavelength low-amplitude (<1 ppm) noise that generates a very rough map (not shown) and was not used in the analysis. Figure 11B and C shows the maps generated by the intermediate and residual filters, respectively.

Many recent studies have been published that deal with fractal filtering of geochemical data (Cheng, 1999; Xu and Cheng, 2001; and references therein). Fractal analysis measures the geometric complexity of map data and how it varies at different scales. Fractal filtering enables one to examine the relationship between the scale of observation and the complexity of patterns observed in a map; thus, these methods can also be used to differentiate and separate patterns that are due to different processes operating at different scales. Cheng (1999) determined that the relationship between the scale of observation and the complexity of map patterns follows a power law and can be expressed as a mathematical function referred to as the power spectrum of a map. The major distinction between the methodology developed by Cheng (1999) and conventional band-pass filtering is that his approach uses irregular wavelength filters, chosen by fractal analysis of the power spectrum of a map.

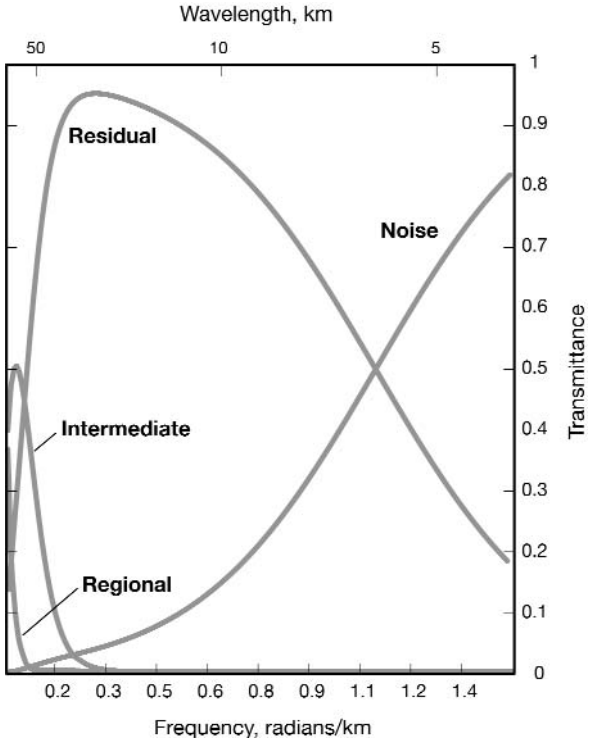

FIG. 10. Wavelength filters used to process the arsenic data. Transmittance means the proportion of the signal at the specified wavelength that is passed (retained) by the filter.

At the time we conducted our modeling, adequate software was not available to process data sets as large as ours by fractal filtering. Since then, we have explored our data with fractal filters and have come to the conclusion that the power spectra of our data are very close to isotropic (radially symmetric). Thus, our band-pass method becomes a special case where the power spectra of our maps are isotropic, and the results we have obtained are closely similar to what would be obtained by fractal modeling. Some geochemical patterns are clearly anisotropic (see, e.g., Cheng, 2001), and we anticipate valuable future research into the relationship of anisotropy to sampling density and other potential parameters of geochemical data sets.

It is not always possible to decompose a map into the three components (regional, intermediate, and residual) as in the arsenic and antimony examples. Many elements lack the large-scale regional gradient, whereas others lack intermediate-scale geochemical structure. It is necessary to experiment with filters until a stable and interpretable result is obtained.

The Example of Arsenic

Old versus new map

Kotlyar et al. (1998) attempted to compensate for known differences between laboratories and analytical methods for arsenic by normalizing the data for each quadrangle before gridding and smoothing. The result was a map that was smooth from quadrangle to quadrangle, unlike the one in Figure 3, which is based on the data as reported. Mihalasky (2001) also studied arsenic distribution in this area. The present study began with the hypothesis that the new data are substantially more useful and better than the original NURE HSSR data for arsenic, and that maps based on the original data might be misleading. Figure 12 is a comparison of the original map (A) from Kotlyar et al. (1998) with a map prepared from our new data (B) using the same gridding methods and the same contour interval.

Although some prominent features can be seen in both maps (e.g., high values in the Independence Mountains and the Battle Mountain-Eureka trend; see Fig. 2), there are important differences throughout the map area, particularly highs that appear only in the earlier map. Examples of this can be seen in the McDermitt and Elko quadrangles (Fig. 4), where the original analyses were by an unknown analytical method. In addition, there are important differences between the old and new maps in the other quadrangles, where the earlier analyses were done by neutron activation methods. For example, the broad high area south of Winnemucca in map A (Fig. 12A) is not present in map B (Fig. 12B), and the area west of Austin is a large and strong anomaly in map A but is much less prominent in map B.

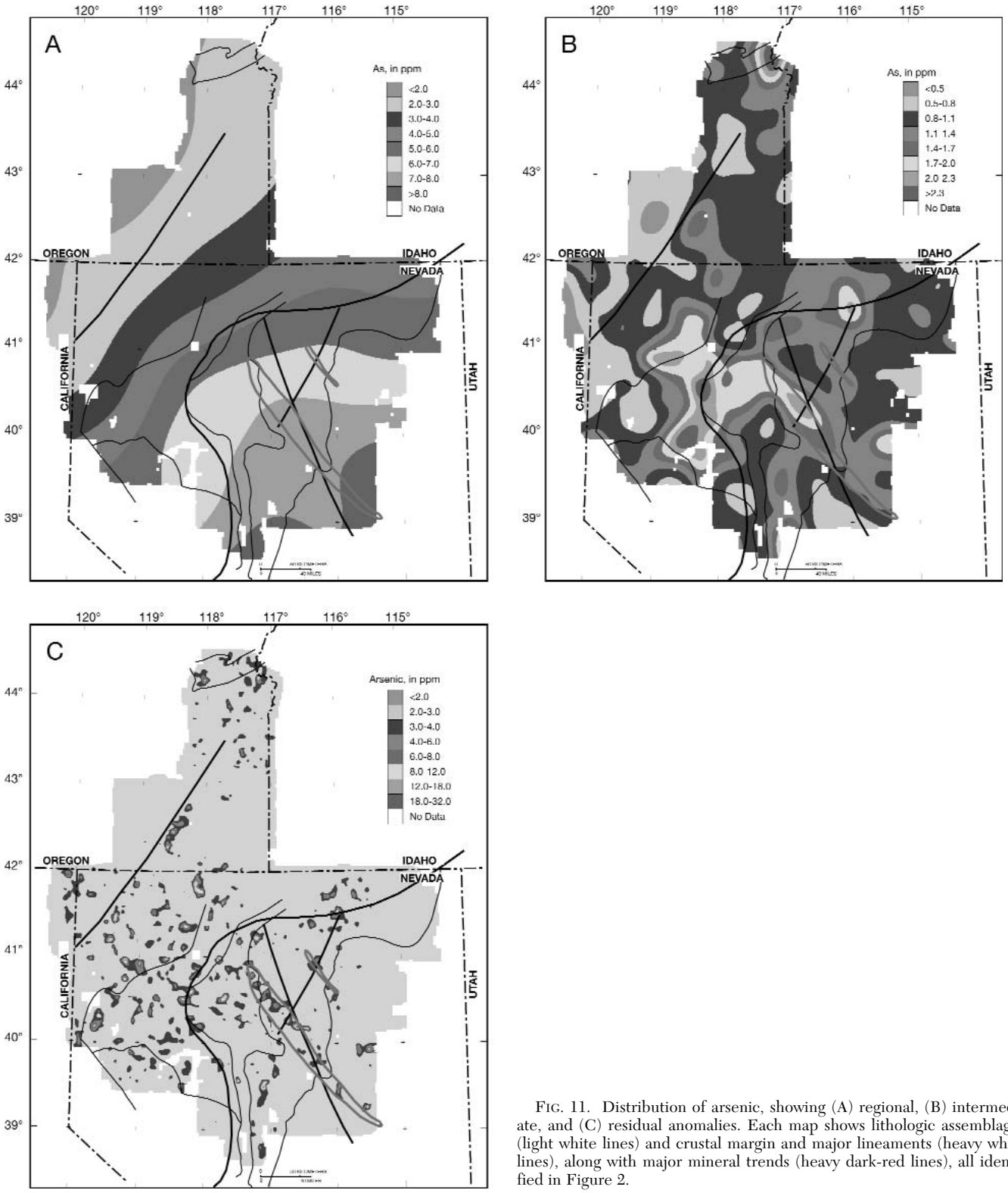

FIG. 11. Distribution of arsenic, showing (A) regional, (B) intermediate, and (C) residual anomalies. Each map shows lithologic assemblages (light white lines) and crustal margin and major lineaments (heavy white lines), along with major mineral trends (heavy dark-red lines), all identified in Figure 2.

Detecting crustal structures

Several features are prominent in Figure 9. Foremost is the observation made earlier, that arsenic concentrations in stream-sediment samples are significantly higher in the southeast half of the map than in the northwest half. Many of the large areas with values greater than 10 ppm can be related to major mineral trends and districts, such as the Battle Mountain-Eureka trend, the Carlin trend, the Independence Mountains

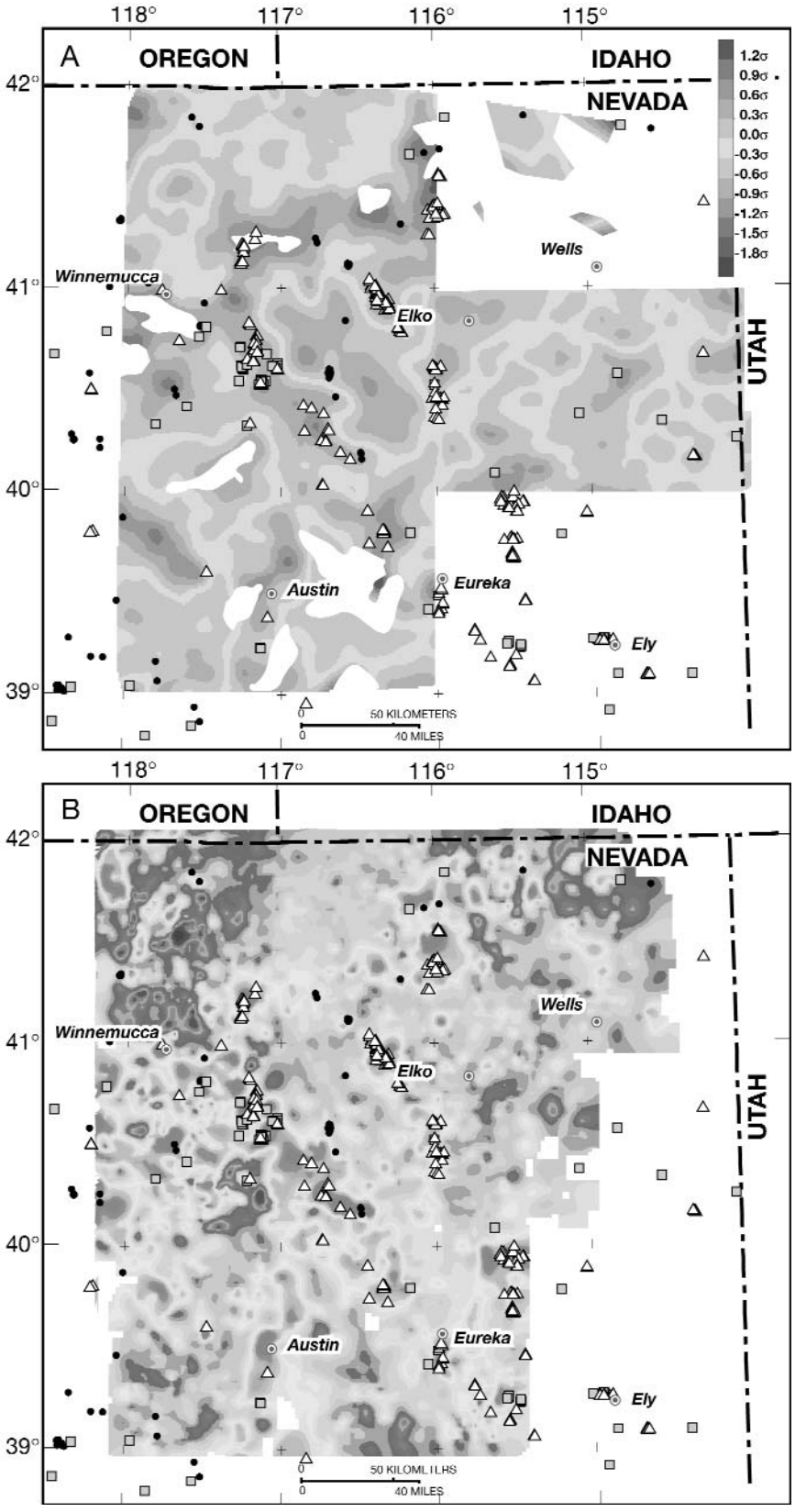

FIG. 12. Maps showing (A) distribution of arsenic based on original NURE analyses using normalized data (Kotlyar et al., 1998) and (B) distribution of arsenic based on new analyses (Coombs et al., 2002). Both maps are contoured in standard deviations. Triangles indicate sedimentary rock-hosted gold deposits, solid circles indicate epithermal precious metal deposits, and shaded squares indicate pluton-related deposits and prospects.

region, the Getchell trend, the Bald Mountain district, the Reese River district near Austin, and the McDermitt area. In addition there is a broad area of high values west of Battle Mountain, nearly 200 km in diameter, which stretches from Winnemucca nearly to Fallon (see Fig. 2 for location of geographic entities not shown in Fig. 9). Superimposed on this larger feature are a number of smaller areas of high values, with dimensions of 5 to 20 km.

The distribution of arsenic in the near-surface environment can reflect a number of different controls. These include primary controls, which might include occurrence in trace sulfides present in many igneous rocks and as possible isomorphous substitution in primary silicate and oxide minerals. Arsenic also can be transported into rocks by subsequent hydrothermal activity and is common in hydrothermal alteration halos. Arsenic is readily dissolved, transported, and redeposited by relatively cold ground waters, flowing through pore spaces or along regional structures. And, finally, it can be dispersed by surface waters, both in particulate form in bed load and in solution.

Primary igneous and sedimentary host-rock controls appear to be largely masked by later events that have redistributed arsenic. Examination of the total spectrum map, overlain by major lithologic assemblage boundaries in the study area (Fig. 9), shows little correlation of the arsenic distribution patterns with lithologic boundaries. The only lithologic boundary that seems to be refelected in the maps is part of the boundary of Miocene volcanic cover in northwest Nevada, where the area underlain by volcanic rocks has distinctly lower arsenic values. This is consistent with the observation discussed earlier that most of the arsenic in the samples is secondary and is adsorbed on Mn-Fe oxides rather than present in sulfides or silicates. The spatial patterns of these elements appear to be largely the result of solution transport; to attempt to characterize map units by their arsenic content would be misleading.

The scale of the hydrothermal systems compared to the sampling density of this study implies that hydrothermal anomalies may encompass only a few data points and result in anomalies in the gridded maps with dimensions of a few to a few tens of kilometers. Many anomalies of this size can be seen in Figures 9 and 11C, and many can be related to known mining districts.

Dunbar et al. (1995) noted significant changes in arsenic levels in ground water flowing through rocks that are relatively rich in arsenic. If transport is over long distances, large structures with dimensions of 100s of kilometers that guide arsenic transport and deposition may be discernible. Some features of this scale are visible in Figures 9, 11A and B and are discussed below.

Transport of arsenic by surface waters may also be important locally. However, especially in the modern arid climate of the Great Basin, stream transport probably is restricted to short enough distances that the maps based on our samples do not show a relationship to drainage systems. Also, because the samples were collected on first- and second-order streams (defined at 1:24,000 scale), there should be little or no evidence of downstream trains of transported arsenic, and we have identified no such patterns on the maps. A first-order stream is the first segment to drain that land area, which has not yet intersected another stream; a second-order stream is formed by the confluence of two first-order streams.

Examination of the arsenic maps (Figs. 9, 11) leads to a number of insights regarding regional structures.

Cratonal margin: The location of the margin of the sialic North American craton places important constraints on the tectonic evolutionary history of the Great Basin and has been an important topic of discussion since its introduction in the early 1970s (Kistler and Peterman, 1973; Kistler, 1974). The strontium isotope composition of Mesozoic and younger plutonic rocks indicates the chemical nature of the underlying crust through which the plutons ascended. In general, plutonic rocks that overlie oceanic crust have $^{87}Sr/^{86}Sr$ initial ratios less than about 0.706, whereas plutonic rocks that overlie sialic craton have higher ratios. The cratonal margin in Figures 9 and 11 was constructed using similar considerations, however here it represents the break in slope of east-west profiles of the isotopic data and lies slightly to the west of the classic "0.706 line." The important observation is that large parts of the Great Basin, to the north and west of this line, are apparently underlain by Mesozoic oceanic crust.

This feature can be mapped using the regional arsenic geochemical data. Figure 9 demonstrates that most high values of arsenic are to the south and east of this line (and over similar cratonal crust in eastern Oregon). In Figure 11A, the cratonal margin corresponds approximately to the 5-ppm contour on the regional map, which isolates the longest wavelength portion of the arsenic variation.

Although it is known that upper continental crust is enriched in arsenic relative to lower and oceanic crust (Rudnick and Gao, 2003), why this is so is not readily apparent. One possible explanation is simply related to time. If arsenic is transported to the upper crust primarily by magmatism and associated hydrothermal activity, then arsenic anomalies should be much more common where the crust is older. Alternatively, if oceanic crust has lower arsenic content than continental crust, magmas and fluids that interact with primarily oceanic crust would transport less arsenic to the surface.

Mineral deposit trends: The Battle Mountain-Eureka trend and the Lynn-Railroad belt (later renamed the Carlin trend in Roberts, 1960) represent the coincidence of a series of windows through the Roberts Mountains allochthon with an unusual concentration of hydrothermal mineral deposits, primarily of Eocene age (Arehart, et al., 2003). They are the most prominent linear patterns in a nationwide map of significant mineral deposits (Long et al., 2000).

The Battle Mountain-Eureka trend is easily discerned in the arsenic maps. It is seen as a series of prominent highs, many corresponding to known deposits and districts, that stretches for at least 250 km from the Winnemucca district northwest of Battle Mountain to southeast of the Eureka district. The relationship of the trend to underlying deep crustal structures, if any, is the subject of continued research. Pertinent discussions include those of Hildenbrand et al. (2000), Grauch et al. (2003), and Howard (2003). Based primarily on geophysical evidence, these authors agree that the mineral deposit trend is close to, but does not correspond exactly with, an important crustal boundary that separates dense material to the northeast and less dense material to the southwest. The mineral deposit trend also extends considerably

farther to the southeast than the geophysical features. We interpret the high arsenic values along this trend to be the result of the introduction of arsenic by hydrothermal fluids related to the Eocene plutons and mineral deposits. The linear arrangement of the anomalies suggests that they may be controlled by a deep fracture zone, but the relationship to the geophysical features remains unclear.

The Carlin trend presents an enigmatic signature in the arsenic maps. Geophysical evidence for a deep crustal structure is equivocal (Hildenbrand et al., 2000; Grauch et al., 2003). Although two prominent arsenic highs correspond with the northern and southern parts of the trend, there is a distinct gap in the central part of the trend, between the Maggie Creek area and the group of deposits near Rain. In this gap, postmineral rocks cover the productive strata, and few deposits and prospects are known at the surface. The result is that, when taken in the context of the entire map, the arsenic geochemical signature of the Carlin trend is not distinctly linear nor is it large and prominent enough to appear in the map of intermediate wavelengths (Fig. 11B). It also does not extend beyond the known limits of mineralization, either to the northwest or to the southeast. See also Mihalasky (2001).

Northern Nevada rift: The northern Nevada rift was first recognized by Philbin et al. (1963) and Mabey (1965, 1966). This feature was later described by Zoback and Thompson (1978) on the basis of a prominent, narrow, positive magnetic anomaly that extends for nearly 500 km in a north-northwest direction from east-central Nevada to near the Nevada-Oregon border (Zoback et al., 1994). It has been interpreted to be the magnetic manifestation of a largely subsurface mafic dike swarm, emplaced along a deep-seated fracture system that cuts all pre-Miocene upper crustal rocks (Mabey, 1965, 1966). Exposed dikes and lava flows are common in the northern part of the feature but less so in the southern part, probably because the top of the dike swarm is deeper in the south (Blakely and Jachens, 1991). A series of similar aeromagnetic features to the west has been identified by McKee and Blakely (1990), and postulated by Glen and Ponce (2002) to be related to processes similar to those responsible for the northern Nevada rift anomaly.

The dikes and lava flows associated with the rift are temporally related to many low-sulfidation epithermal precious metal deposits, all formed between about 16 and 14 Ma (Wallace and John, 1998; John and Wallace, 2000; Ponce and Glen, 2002). This time interval also corresponds to the postulated inception of the Yellowstone hot spot (Thompson and Gibson, 1991; Zoback et al., 1994; Pierce et al., 2000). The rocks are mostly tholeiitic basalts and basaltic andesites, typical of the mafic rocks of the bimodal basalt-rhyolite assemblage of Ludington et al. (1996a).

Despite the probability that it served as a magmatic conduit, the rift and its possible western affiliates are not associated with apparent arsenic anomalies (Fig 11C). We believe this is evidence that the northern Nevada rift structure, whatever its nature, was active over only a short time interval. Although it apparently served as the pathway for magma emplacement during a short period between 16 and 14 Ma, it was apparently not a conduit for subsequent regional fluid circulation, although low-sulfidation epithermal precious metal deposits formed during the same time period (Wallace and John, 1998). Interestingly, the deposits associated in time and space with the rift also are not obviously associated with arsenic anomalies (Fig. 11C). Of 16 low-sulfidation deposits in northern Nevada that apparently formed in the 16 to 14 Ma time interval, 11 have no arsenic anomaly, whereas only five do, and several of those are relatively weak. Whether this lack of a dispersed arsenic anomaly is a general characteristic of low-sulfidation deposits is unclear.

Other features: A feature called the Crescent Valley-Independence lineament has been proposed recently by Peters (1998) and suggested to be a major fluid conduit related to sedimentary rock-hosted deposits. The lineament extends from the Independence mining district in the north to near the Cortez mine in the south, passing through the central part of the Carlin trend. This feature appears to reflect mainly compressional features developed before the Jurassic. There are no features (anomalies or offsets) in the arsenic maps (Figs. 9, 11) that can be related to this feature, and it seems unlikely that it was a conduit for arsenic or other metals.

The feature named here as the Steens lineament (Figs. 2, 9, 11) is associated with high arsenic values that extend N30E for more than 200 km. In the total spectrum map (Fig. 9), it corresponds to the linear part of the 3 ppm contour, with values all less than 3 ppm to the northwest of the line. In the intermediate map (Fig. 11B), the lineament corresponds to the northwest boundary of two broad positive anomalies, one in southeast Oregon and one in northwest Nevada. In the residual map (Fig. 11C), it is marked by a series of six residual anomalies that occur along its eastern edge. Thus, a series of discontinuities in arsenic distribution patterns, rather than a linear positive anomaly, indicates the lineament, which corresponds to a number of tectonic features.

At Steens Mountain, this lineament corresponds to the Alvord fault, which has Holocene movement, and which is part of the northeast-trending Steens fault zone (Hemphill-Haley et al., 2000). This fault zone has been extended to the northeast by Lindberg (1989). In addition, the trace of the lineament corresponds to numerous normal faults compiled in the geologic maps of Oregon (Walker and MacLeod, 1991) and Nevada (Stewart and Carlson, 1978).

The lineament lies a few kilometers to the northwest of the Black Rock structural boundary, as delineated by Rytuba et al. (1991). Northwest of this boundary, outcrops of Paleozoic and Mesozoic rock are not present, and the area is believed to now consist of newly generated Miocene and younger crust that formed in response to the continued clockwise rotation of the tectonic block to the south. This model, first proposed by McKee et al. (1990), is also supported by recent studies of gravity in the area (Jachens and Moring, 1990; Hildenbrand et al., 2000).

Taken together, this evidence supports a model for the Steens lineament as a normal fault zone, active since the Miocene, primarily after emplacement of the Steens Basalt (shortly after 16 Ma) that is controlled by a deeper feature in the crust. This zone may have served to localize the ascent of magmas and accompanying hydrothermal fluids that have repeatedly transported arsenic to the surface.

Regional heat flow

In addition to the structures described above, the spatial distribution of arsenic values points to a different, broad

feature in northwest Nevada. The intermediate-wavelength map (Fig. 11B) displays a broad northeast elongate area of high arsenic values that is located to the west of the Battle Mountain-Eureka trend. This feature is spatially correlated with several features, all related to young (post-14 Ma) faulting, extension, and high heat flow, without extensive accompanying volcanism. Within, or very close to, the anomalous areas are most of a distinctive group of epithermal precious metal deposits that are post-Miocene in age and do not appear to be related directly to volcanism, including Florida Canyon, Sulphur, Relief Canyon, and Dixie Comstock. The area also encloses five of the ten active geothermal plants in Nevada, as well as a concentration of hot springs and other geothermal features (Hess, 2001; Shevenell and Garside, 2003).

Environmental implications of arsenic distribution

The Great Basin is well known for high arsenic in ground water (Focazio et al., 1999; Welch et al., 2000). The composition of surficial materials may affect the composition of ground water, and, if arsenic contents are high enough, the materials themselves may be characterized as hazardous. However, existing data about arsenic in ground water in the study area is too sparse to permit speculation about possible correlations with arsenic in surficial materials.

A brief survey of national- and state-proposed remediation goals for arsenic in surficial materials indicates levels of concern that range from less than 2 ppm to several hundreds of ppm. By comparison, the smoothed values for arsenic in broad areas of the Great Basin exceed 20 ppm (Fig. 9). Because the samples were collected in the 1970s, this distribution does not reflect effects that may be due to the large-scale mining that has taken place in the past 30 years. Most of the region characterized by the highest arsenic values is generally remote from any densely populated areas. It is also important to note that most of the arsenic depicted in this map is probably adsorbed on Mn-Fe oxide particles and thus not amenable to leaching by rainwater or other surface waters.

Arsenic and mineral deposits

Although the gradient and regional baseline maps provide important information about Great Basin metallogeny, the primary tool to indicate gold-bearing mineral deposits is the residual arsenic map (Fig. 11C). Arsenic is widely regarded as a pathfinder element for gold deposits in the region. The residual map contains 162 distinct anomalies above the 3 ppm level. Here, we compare the distribution of anomalies to that of known metallic mineral districts (Tingley, 1992) and significant base and precious metal deposits (Long et al., 2000).

Of the 162 anomalies, 95 of them (about 59%), are spatially associated with (i.e., intersect) known metallic mineral districts. Because there is no authoritative compilation of mineral districts for Oregon, this percentage could be larger. A number of the anomalies in eastern Oregon are near important epithermal gold deposits and prospects in areas without well-defined historic mining districts. The great majority of the anomalies not associated with known districts and deposits are located northwest of the inferred craton margin and, perhaps more importantly, in regions where the bedrock is Miocene and younger volcanic rock. Although this region is characterized by lower background arsenic values, district-scale anomalies appear to be as common as they are in areas of older exposed bedrock to the south and east (Fig. 11C). This pattern supports the idea that arsenic and arsenic-mineralized areas do not commonly survive over long periods of geologic time. That is to say, it is unlikely that many of the residual anomalies in the south and east parts of the study area were formed prior to the Tertiary. The pattern also suggests that the northern region has been underexplored for gold deposits.

Of the 221 metal mining districts within the study area, 91 of them (41%) are associated with arsenic anomalies, whereas 131 (59%) are not. We make no generalizations about the districts without arsenic anomalies; they include deposits of a wide variety of types, including some large and important ones. Some notable epithermal deposits and districts not associated with arsenic anomalies include Bruner, Olinghouse, Rosebud, Gold Circle (Midas), National, and Argenta (Mule Canyon), in Nevada, and Grassy Mountain, Oregon. In addition, sedimentary rock-hosted deposits such as Gold Quarry, Illipah, Austin Gold Venture, Fondaway Canyon, Bootstrap, Dee, and Rossi have no apparent arsenic signature. Of the 91 districts with an arsenic association, 53 (58%) contain only deposits that do not qualify as significant by the criteria of Long et al. (2000). Sixteen districts contain significant epithermal deposits, 19 contain significant sedimentary rock-hosted or distal-disseminated precious metal deposits, and 12 contain important pluton-related deposits or prospects. Among the low-sulfidation epithermal deposits that are the same age as igneous rocks related to the northern Nevada rift (see Wallace and John, 1998; Ponce and Glen, 2002), more than two-thirds are not associated with an arsenic anomaly.

To summarize, there is a strong association of district-scale arsenic anomalies with hydrothermal base and precious metal deposits. A number of very large deposits, however, have no arsenic anomalies, and a large number of arsenic anomalies are not associated with known mineral deposits. Arsenic appears to be less well correlated with epithermal deposits than with other types of deposit. There are many reasons why a particular deposit will not produce a prominent geochemical signature. Among the most obvious are postmineral cover and the failure to detect a mineralized system because of inopportune sampling sites and stream patterns. These likely explain some of the deposits and districts not associated with arsenic anomalies, but to evaluate each one is beyond the scope of this study. Nevertheless, some further observations can be made about the spatial distribution of the residual anomalies shown in Figure 11C.

First, neither the linear nature nor the importance of the Carlin trend is indicated by the arsenic anomaly patterns. This is a good example of how postmineral cover, which is prevalent both at the far north end and in the central part of the trend, can conceal potential geochemical anomalies.

On the other hand, the Battle Mountain-Eureka trend corresponds to a prominent linear arsenic anomaly, consisting of a series of at least 12 separate anomalies centered in the trend. Here, a sufficient number of the mineralized systems are exposed at the surface to clearly indicate the geometry of the trend. The Steens lineament is also prominent, indicated by at least six anomalies distributed along its length on the

southeast side. There are no arsenic anomalies to indicate the location of the northern Nevada rift or of the Crescent Valley-Independence lineament.

Principal Component Analysis

To take advantage of correlations among the 21 different elements in the data set, we chose a traditional approach using the R-mode factor analysis package in the commercial program STATVIEW to simplify the analysis of the relationships among the variables. This evaluation produces a smaller set of new variables called factors (or principal components) that contain the essential information in the data set. The results are summarized in Tables 2 and 3.

Data for all 21 elements was transformed to base 10 logarithms before calculations. The correlation matrix is an important input to the factor analysis, and it is shown as Table 2. The components were rotated using the Varimax method. We calculated six factors for this study, and they are listed in Table 3. The six factors account for 78 percent of the total variance in the data set. The factor score for each sample is calculated by summing the product of the loadings or weights shown in Table 3 multiplied by the corresponding geochemical values. The factor scores for each sample can then be plotted on maps. We have interpreted the spatial distribution of only the first two factors, which together account for 49 percent of the variance. The distributions of the loadings for the first two factors are discussed separately below.

The strongest factor: basalt

Factor 1, which explains 27 percent of the variance in the data set, is associated with a specific igneous rock type, alkaline basalt. This factor has strong positive loadings >0.5 for Fe, Ti, V, Cu, Ni, and Zn, reflecting mafic igneous rock compositions. Figure 13 shows the distribution of the highest scores for factor 1, compared to the distribution of Miocene basaltic rocks. There is a strong correspondence between the two features; almost all the areas with high loadings for factor 1 are in or very near regions of Miocene basaltic rocks. Some areas of basaltic rocks do not correspond to high scores for factor 1. This may be due to incomplete sampling in some cases, but more likely it is because of variations in basalt composition. There are a few areas with high factor 1 scores that are not near known basaltic rocks; the explanation for these anomalies is not known, but it could be due to basalt outcrops too small to portray in the 1:500,000 state geologic maps used for this study.

The elements in this factor with positive loadings are relatively immobile (except for zinc). Although we filtered these data and looked for short-wavelength information, the resulting maps showed an apparently random pattern of very low amplitude anomalies. We concluded that there is no important short-wavelength variation in this factor and that the patterns are due primarily to bedrock lithology.

In Figure 13, the most prominent area with high scores for factor 1 corresponds to exposures of the Steens Basalt (Gunn and Watkins, 1970; Carlson and Hart, 1983). Widely exposed throughout southeastern Oregon, this distinctive 16.6-Ma basalt represents the remnants of a Miocene shield volcano that may have been 100 km in diameter (Mankinen et al., 1987; Johnson et al., 1998). These basalts are the same age and generally the same composition as those of the Columbia River basalt province.

The Steens basalts are, like many other basalts from the northern Great Basin (Fitton et al., 1991), distinct from oceanic island basalts, in that they have distinctly lower La/Ba and somewhat lower La/Nb (data from Johnson et al., 1998).

TABLE 3. Loadings for Six Strongest Factors Identified in Principal Component Analysis of Stream-Sediment Samples from the Northern Great Basin

Factor one		Factor two		Factor three		Factor four		Factor five		Factor six	
Fe	**0.88**	**Sb**	**0.77**	**Ce**	**0.87**	**Ca**	**0.77**	**Ba**	**0.90**	**Au**	**0.62**
Ti	**0.82**	**Ag**	**0.77**	**La**	**0.84**	**Sr**	**0.69**	Sr	0.14	Na	0.41
V	**0.82**	**As**	**0.75**	**Th**	**0.66**	**Mg**	**0.54**	K	0.14	Sr	0.24
Cu	**0.64**	**Pb**	**0.67**	K	0.45	Na	0.28	V	0.09	Ag	0.21
Ni	**0.64**	**Au**	**0.63**	Y	0.38	As	0.22	As	0.07	Ti	0.16
Zn	**0.50**	**Zn**	**0.53**	Pb	0.31	V	0.13	Ni	0.06	Fe	0.11
Y	0.40	Cu	0.26	Ti	0.19	Sb	0.12	Zn	0.04	K	0.08
Mg	0.30	Mg	0.24	Na	0.18	Th	0.07	La	0.02	V	0.07
Ce	0.21	Ni	0.19	Fe	0.15	Fe	0.04	Th	0.02	Y	0.06
Ba	0.08	Th	0.16	As	0.11	La	0.01	Ti	0.01	Sb	0.04
Pb	0.07	K	0.12	Zn	0.10	K	–0.01	Sb	0.01	Ba	–0.01
Na	0.05	Ca	0.10	Ba	0.07	Ti	–0.01	Cu	–0.01	As	–0.02
Au	0.03	La	0.10	Sb	0.01	Ag	–0.04	Ag	–0.02	Th	–0.03
Sr	0.03	Ba	0.00	Sr	0.01	Ni	–0.04	Ce	–0.05	Zn	–0.04
La	0.02	Ce	–0.03	Ag	–0.01	Ba	–0.05	Au	–0.05	Cu	–0.05
Ca	0.01	V	–0.03	V	–0.03	Ce	–0.06	Fe	–0.05	Pb	–0.05
Sb	–0.06	Fe	–0.14	Ca	–0.11	Zn	–0.09	Na	–0.07	Ce	–0.07
Ag	–0.08	Sr	–0.25	Mg	–0.13	Au	–0.10	Mg	–0.12	La	–0.08
As	–0.09	Y	–0.29	Au	–0.16	Pb	–0.13	Pb	–0.14	Ca	–0.12
Th	–0.22	Ti	–0.39	Ni	–0.16	Cu	–0.14	Ca	–0.15	Mg	–0.25
K	–0.39	***Na***	***–0.53***	Cu	–0.21	Y	–0.37	Y	–0.26	Ni	–0.26
% var	27.3%		21.5%		13.3%		7.5%		4.3%		4.0%
% of	tot var		48.8%		62.1%		69.6%		73.9%		77.9%

Notes: Original data for Ag, As, Cu, Pb, Sb, and Zn were partial extraction analyses; original data for Ca, Fe, K, Mg, Na, and Ti, were in percent, the rest in ppm; factor loadings ≥0.5 shown in bold type for emphasis; factor loadings ≤–0.5 shown in bold italic type

TABLE 2. Correlation Matrix of Elemental Concentrations in Stream–Sediment Samples from the Northern Great Basin

As	**0.50**																								
Au	**0.51**	0.39																							
Ba	0.22	0.29	0.12																						
Ca	–0.11	0.01	–0.04	–0.12																					
Ce	–0.03	–0.01	–0.09	0.13	–0.41																				
Cu	0.19	0.17	0.22	–0.05	0.14	–0.26																			
Fe	–0.20	–0.15	–0.02	–0.17	0.19	0.02	**0.51**																		
K	0.15	0.21	0.01	0.28	–0.44	0.44	–0.44	***(–0.50)***																	
La	0.13	0.11	–0.01	0.23	–0.40	**0.91**	–0.36	–0.18	**0.57**																
Mg	0.02	0.14	0.07	–0.09	**0.66**	–0.41	0.47	0.42	–0.44	–0.44															
Na	***(–0.50)***	–0.45	–0.31	–0.21	0.14	0.08	–0.23	0.21	0.07	–0.05	–0.07														
Ni	0.12	0.15	0.15	0.00	0.22	–0.22	**0.74**	**0.52**	–0.48	–0.31	**0.57**	–0.28													
Pb	**0.57**	0.47	0.31	0.17	–0.28	0.30	0.18	–0.12	0.25	0.35	–0.10	–0.46	0.09												
Sb	**0.58**	**0.73**	0.41	0.23	–0.01	–0.08	0.21	–0.12	0.11	0.03	0.13	–0.48	0.18	0.49											
Sr	–0.28	–0.19	–0.18	0.04	**0.64**	–0.24	–0.05	0.20	–0.24	–0.26	**0.58**	–0.05	–0.43	–0.23											
Th	0.16	0.16	0.02	0.19	–0.40	0.60	–0.39	–0.31	**0.65**	**0.72**	–0.42	–0.04	–0.40	0.28	0.07	–0.23									
Ti	–0.35	–0.37	–0.16	–0.14	0.16	0.11	0.37	**0.83**	–0.44	–0.10	0.25	0.39	0.36	–0.22	–0.31	0.29	–0.31								
V	–0.08	–0.03	0.06	–0.05	0.34	–0.19	**0.62**	**0.84**	***(–0.57)***	–0.32	**0.55**	0.07	**0.65**	–0.17	0.02	0.28	–0.40	**0.73**							
Y	–0.24	–0.29	–0.17	–0.18	–0.30	0.46	0.03	0.27	0.06	0.28	–0.27	0.22	–0.04	0.02	–0.25	–0.23	0.09	0.38	0.04						
Zn	0.47	0.36	0.30	0.16	0.01	0.00	**0.53**	0.35	–0.12	0.01	0.25	–0.42	0.44	**0.50**	0.40	–0.23	–0.06	0.13	0.39	–0.03					
	Ag	As	Au	Ba	Ca	Ce	Cu	Fe	K	La	Mg	Na	Ni	Pb	Sb	Sr	Th	Ti	V	Y					

Notes: Original data for Ag, As, Cu, Pb, Sb, and Zn were partial extraction analyses; original data for Ca, Fe, K, Mg, Na, and Ti were in percent, the rest in ppm; positive correlation coefficients ≥0.5 shown in bold type for emphasis; nNegative correlation coefficients ≤0.5 shown in bold italic type and in parentheses

The Cu and Ni contents of Steens Basalt are high. Gunn and Watkins (1970) report Ni values from 49 to 114 ppm and Cu values from 136 to 342 ppm and stated that small grains of sulfide minerals are present in many of the basalts. The extensive data presented by Johnson et al. (1998) are reported for two stratigraphic units; the lower unit has Ni values from 50 to 345 ppm and Cu values from 84 to 234 ppm. These data, combined with the distribution of high scores for factor 1 in Figure 13, suggest that there are significant variations in the trace element composition within the overall group of Steens-type basalts, as defined by Hart and Carlson (1987).

A detailed inspection of the stream-sediment samples in the Steens Mountain area shows that the highest scores for factor 1 are associated specifically with the lower part of the Steens Basalt sequence. This supports the observations of Johnson et al. (1998) that the Cu- and Ni-rich parts of the Steens Mountain section are uniformly at the base of the sequence.

Aside from the Steens Mountain area, other locations with high factor 1 scores include parts of the Strawberry Volcanics, west of Vale, Oregon, the Bilk Creek Mountains, southeast of Denio, Nevada, areas along the west side of Smoke Creek Desert, near the border with California, west of Gerlach, Nevada, the Goldbanks Hills, south of Winnemucca, Nevada, and the northern Stillwater Range, east of Lovelock, Nevada. These basalts appear to be distinctive and could be considered Steens-like in the sense proposed by Hart and Carlson (1987). Certainly, they are relatively high in Cu, Ni, and Zn. The Miocene basalts associated with the northern Nevada rift do not have high factor 1 scores; they presumably lack the chalcophile element enrichment shown by the Steens-like rocks. The correlations suggested here are in agreement with those proposed by Mankinen et al. (1987) but extend the occurrence of Steens-like rocks farther to the south, into central Nevada.

The hydrothermal mineralization factor

Factor 2, which accounts for nearly 22 percent of the variance in the data set, represents diverse hydrothermally mineralized rocks. This factor has strong positive loadings >0.5 for Sb, Ag, As, Pb, Au, and Zn, and a strong negative loading >0.5 for Na.

The map of factor 2 scores was filtered in an analogous way to the arsenic map described earlier, using band-pass wavelength filters. We were unable to produce a stable intermediate-avelength map (unlike with arsenic) and have interpreted only the short-wavelength, residual map. Figure 14 shows the distribution of the residual anomalies for factor 2, compared to significant hydrothermal mineral deposits and mining districts. Figure 14 also shows the shape of the regional background map that was removed to obtain the residual map. This regional background bears a strong spatial resemblance to the regional arsenic map (Fig. 11A), with low values in the northwest part of the map and high values in the southeast part, over the craton. The residual anomaly map is also similar to maps for the other individual elements that have high loadings for factor 2. The gold map (Coombs, 2002), for example, shows many of the same highs, but because so many of the determinations for gold are below the detection limit, the gold map tells us little about variations in the background.

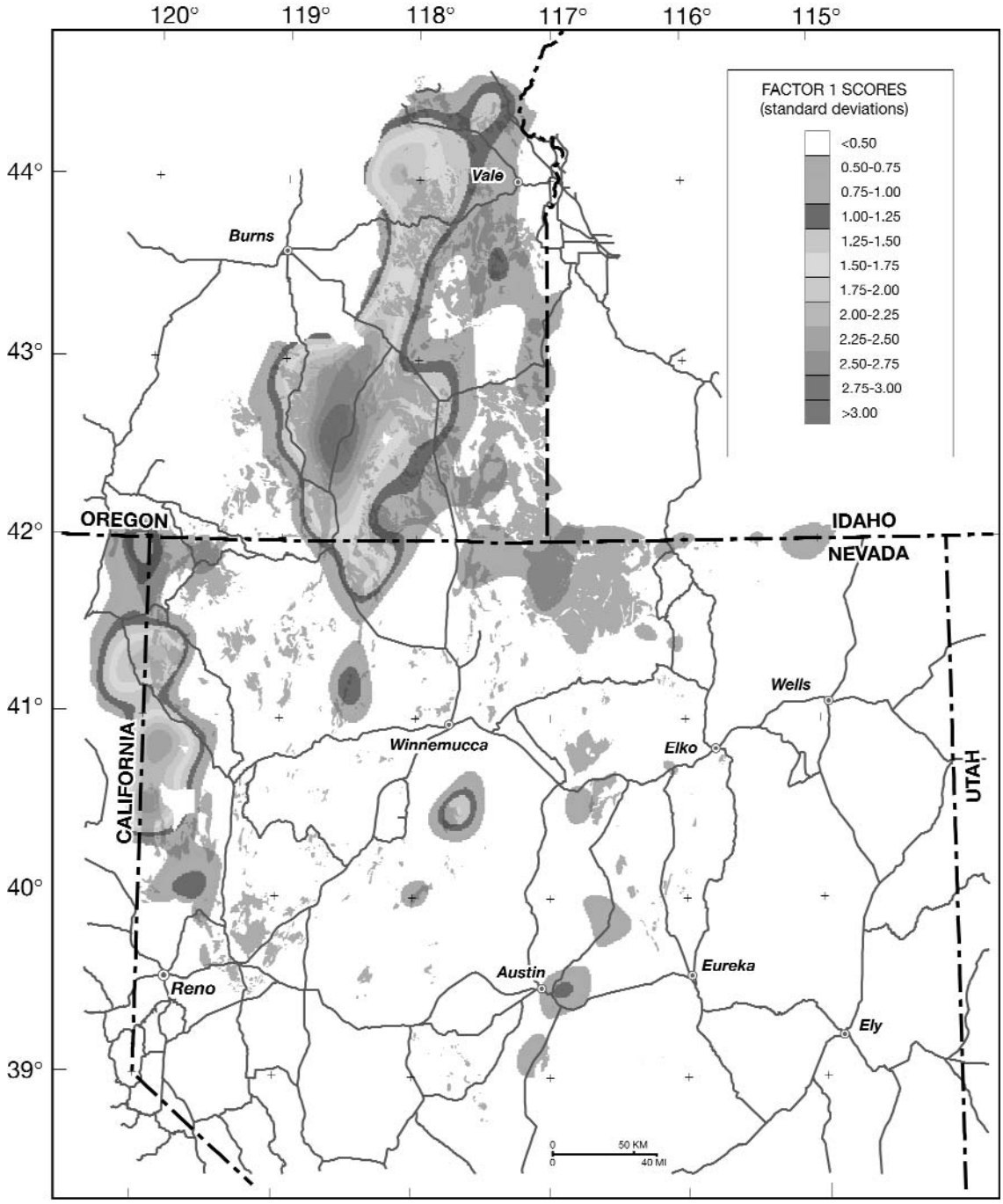

FIG. 13. Map showing distribution of high scores for factor 1 (strong positive loadings >0.5 for Fe, Ti, V, Cu, Ni, and Zn), which are indicative of mafic igneous rocks, compared to the distribution of Miocene mafic volcanic rocks, shown in solid orange. This unfiltered map apparently contains little or no important short-wavelength information. The volcanic rock outcrops are based on the digital geologic maps of Nevada, California, Oregon, and Idaho (Johnson and Raines, 1996; Saucedo et al., 2000; Miller et al., 2003; Raines et al., 2003).

There is a strong correspondence between high scores for factor 2 and known mineral deposits. All the most important sedimentary rock-hosted deposits correlate with residual anomalies for factor 2. This includes the deposits of the Carlin trend, the Battle Mountain-Eureka trend, the Independence Mountains, and the Getchell trend, as well as the Bald Mountain and the Big Creek districts (Austin Gold Venture). Among pluton-related deposits, the Battle Mountain, Eureka, Contact, and White Pine districts, and the McCoy-Cove deposit are prominent. Epithermal deposits and districts associated with factor 2 anomalies include Tuscarora, Midas, Sulphur, Hog Ranch, Trinity Silver, and the Seven Troughs district. Some important districts with mixed or uncertain relationship to factor 2 scores include Austin (Reese River district), New

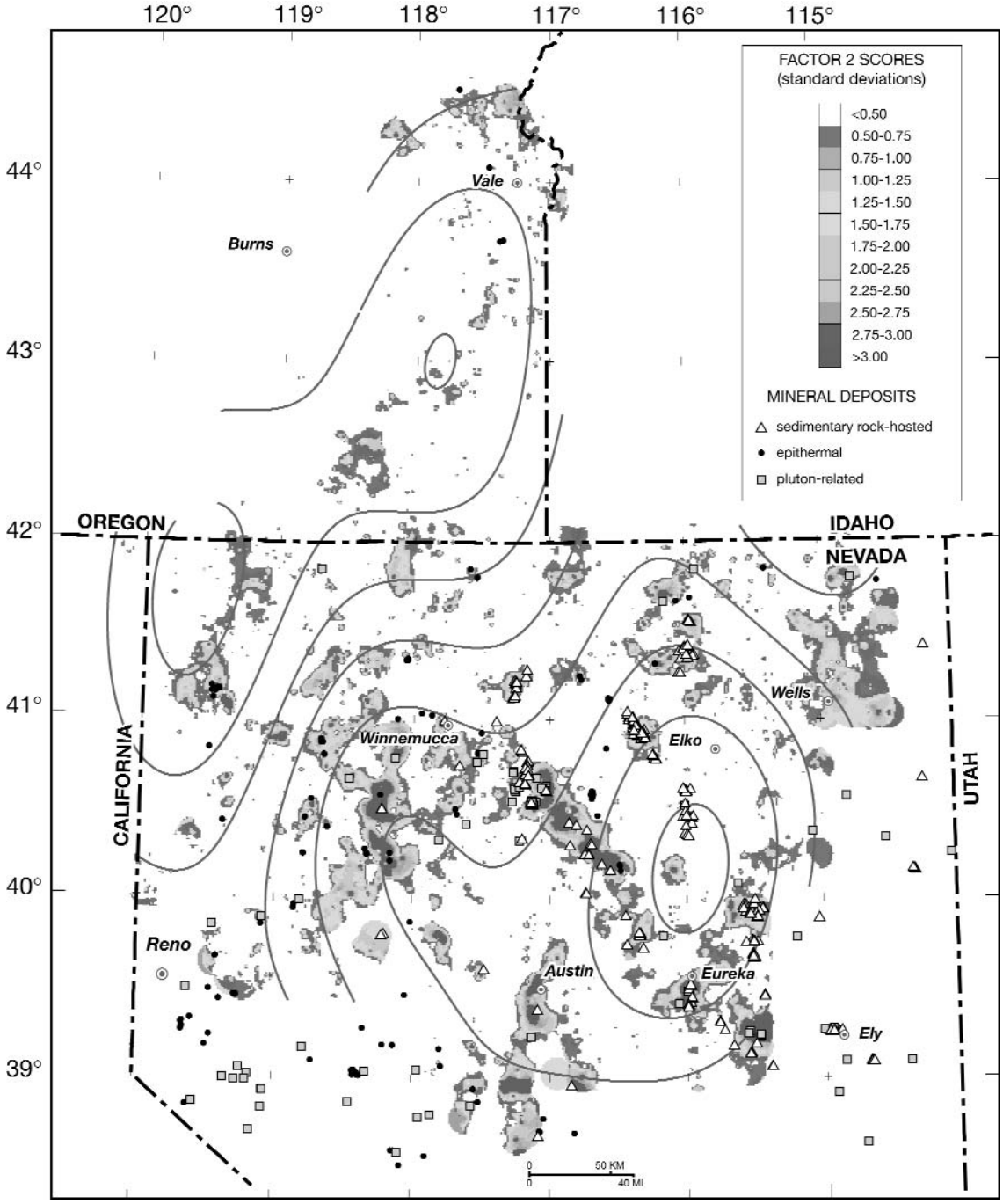

FIG. 14. Map showing the distribution of residual anomalies of factor 2 scores. Factor 2 has strong positive loadings >0.5 for Sb, Ag, As, Pb, Au, and Zn and is indicative of hydrothermally mineralized rock. The map is coded in units of standard deviations, with no pattern for the areas below the mean. Superimposed contours depict the background signal that was removed from the total spectrum.

Pass, and the group of mineral deposits in the West Humboldt range (Florida Canyon, Standard, Nevada-Packard, Relief Canyon, and the Imlay, Rye Patch, and Rochester districts). At least 20 more deposits and districts of lesser importance correspond to anomalies in the factor 2 map (Fig. 15A).

There are some notable deposits that are not indicated by factor 2 (Fig. 15B), the majority being epithermal. Some of the deposits (Redline, Buffalo Valley Mo) do not show a correlation because the deposits are completely covered by postmineral rocks or sediments. Others may have been missed because of irregularities in the sampling array, but many of the deposits not highlighted by factor 2 are relatively small and unimportant. Among the sedimentary rock-hosted gold deposits not associated with high scores for factor 2 are Rain, Marigold, Alligator Ridge, and the Robinson Mountain district. These are all small deposits. Ivanhoe, Mule Canyon,

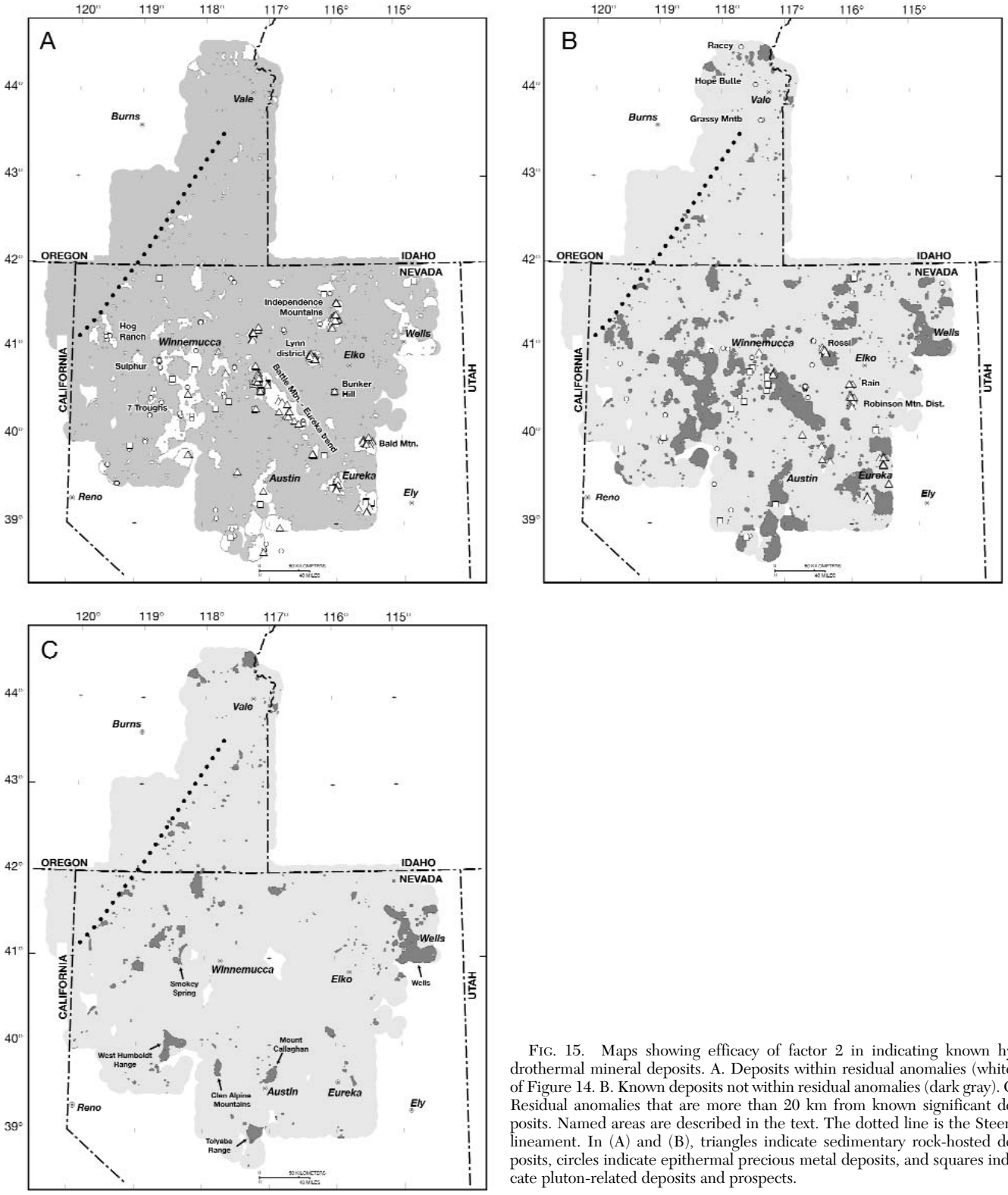

FIG. 15. Maps showing efficacy of factor 2 in indicating known hydrothermal mineral deposits. A. Deposits within residual anomalies (white) of Figure 14. B. Known deposits not within residual anomalies (dark gray). C. Residual anomalies that are more than 20 km from known significant deposits. Named areas are described in the text. The dotted line is the Steens lineament. In (A) and (B), triangles indicate sedimentary rock-hosted deposits, circles indicate epithermal precious metal deposits, and squares indicate pluton-related deposits and prospects.

Fire Creek, Wind Mountain, Mountain View, and the Velvet district are notable epithermal precious metal districts that are not associated with high scores for factor 2.

Perhaps of greater interest are the areas that have high residual scores for factor 2 but are not near important known deposits (Fig. 15C). Such areas can be reasonably viewed as exploration frontiers, where the probability of discovery of new deposits may be high.

In order to demonstrate the utility of the factor 2 maps for regional reconnaissance level prospecting, we have chosen six

areas from those indicated in Figure 15C to highlight. In addition to their prominence on the factor 2 residual map (Fig. 14), these areas all contain three or more individual samples with factor 2 scores more than 2σ above the mean, and they are all more than 20 km away from the nearest known significant deposit.

The largest area surrounds the town of Wells, Nevada, and is underlain primarily by Paleozoic sedimentary rocks. Known mineral deposits include bedded barite deposits and a number of small precious metal-bearing veins. The geochemical signature is complex but includes positive anomalies for Au, Ag, As, Sb, Cu, Pb, Zn, and Ba, as well as marked negative anomalies for Na and K. This signature is found in other rocks of the Roberts Mountain assemblage (Ludington et al., 1996b) and is suggestive of sedimentary exhalative and sedimentary rock-hosted deposits.

The Smokey Spring area, about 60 km west of Winnemucca, is underlain by Permian through Jurassic sedimentary and volcanic rocks. There are very few known mineral deposits in the area. Anomalous elements include Au, As, Sb, Cu, Pb, Zn, Bi, and Ba, and the geochemical signature is again suggestive of sedimentary exhalative and sedimentary rock-hosted deposits.

The West Humboldt Range area, about 80 km northeast of Reno, consists mostly of Triassic and Jurassic sedimentary rocks in the Jungo assemblage of Ludington et al. (1996b). Prominent mineral deposits in this area include bedded gypsum and Sb-Pb-Ag vein deposits. The geochemical signature is dominated by arsenic and antimony, but prominent and extensive anomalies of calcium and molybdenum also characterize the area. This signature is unique and not specifically indicative of any known deposit type.

The anomalous area in the Clan Alpine Mountains, about 60 km west of Austin, coincides with a fault-bounded exposure of Triassic shale and siltstone in a range that otherwise consists primarily of Tertiary volcanic rocks. Most known mineral deposits are distinctive antimony-rich polymetallic veins. Like the West Humboldt area, arsenic and antimony are the most prominent geochemical anomalies, and antimony-rich vein deposits are present, although there appears to be no calicum or molybdenum anomaly.

The Mount Callahan area, immediately northeast of Austin, exhibits complex geology, consisting mostly of Paleozoic sedimentary rocks. Most of the area has few known mineral deposits. The geochemical signature is primarily one of arsenic, antimony, and gold and is moderately suggestive of sedimentary rock-hosted deposits.

The area in the Toiyabe Range, about 50 km southwest of Austin, is underlain by a variety of Paleozoic sedimentary and volcanic rocks and is intruded by three large Mesozoic or early Tertiary granitic plutons. The area contains a number of small polymetallic vein deposits that produced small amounts of precious metals in the middle part of the 19th century. The geochemical anomalies match the trace element geochemistry of the deposits, with strong gold, copper, and lead anomalies, along with lesser concentrations of silver, arsenic, and antimony. This area contains some of the highest gold values in the entire data set, with four samples containing more than 50 ppb gold.

Summary and Conclusions

The study of a large data set of high-quality stream-sediment and soil analyses for the northern Great Basin provides new insights into the geochemistry of geologic features in the area ranging in size from a few to hundreds of kilometers. Although the data were obtained by the analysis of samples collected by various protocols, the resulting data can be interpreted to reveal important information about the upper part of the crust. Depending on the nature of the spatial distribution of values for a particular element, which is a function of the geologic processes by which the element becomes fixed at the surface, either traditional statistical methods of anomaly analysis or more sophisticated methods to model and remove background may be most appropriate to extract the maximum amount of information from the geochemical data.

The modeling methods used here, based on interpolation of data points to create surfaces, followed by deconvolution of the spatial wavelength structure to form maps of varying degrees of smoothness, permit separation of the geochemical signal into maps that show large regional features, as well as mineral district-scale features. Using arsenic, an extremely mobile element, as an example, we have shown the following: (1) the part of the study area underlain by continental crust has a baseline arsenic content nearly an order of magnitude greater than the part underlain by oceanic crust; (2) some linear features, like the Steens lineament and the Battle Mountain-Eureka trend, have been the site of repeated influx and deposition of arsenic by hydrothermal systems related to magmas that ascended along the postulated underlying tectonic features; and (3) other linear features, like the Northern Nevada rift and the Crescent Valley-Independence lineament, while they may have been zones of weakness that helped localize the emplacement of igneous rocks, have not been the sites of arsenic deposition.

There is a strong association of district-scale arsenic anomalies with hydrothermal base and precious metal deposits. A number of very large deposits, however, are not related to arsenic anomalies, and a large number of arsenic anomalies are not associated with known mineral deposits. Arsenic data alone cannot be used to detect specific types of mineral deposits.

Additional analysis of the multielement data using principal components analysis has identified two prominent factors in the data set. The most prominent factor is characterized by Fe, Ti, V, Cu, Ni, and Zn. Mapping of this factor allowed the identification of a number of basalt outcrops in the northern part of the Great Basin that are similar to the Steens Basalt and their separation from outcrops of other, less distinctive Miocene and younger basalts in the region.

Another prominent factor is characterized by high Sb, Ag, As, Pb, Au, and Zn and shows a close relationship to hydrothermal base and precious metal deposits. The map of this factor, like that of arsenic, was deconvoluted into a smooth regional map and a residual map of district-size anomalies. Many of the anomalies on the residual map correspond closely to known mineral deposits in the area. In addition, the anomalies that do not correspond to known deposits could be targets for exploration.

The deconvolution of the spatial wavelength structure of geochemical maps, combined with the use of large regional geochemical data sets, enhances the use of stream-sediment geochemistry, particularly in the study of large-scale crustal features as well as the isolation of mineral district-scale anomalies.

Acknowledgments

Discussions and study with Qiuming Cheng and his graduate students and with Graeme Bonham-Carter have been extremely useful in maintaining enthusiasm for spatial wavelength methods. Gary Raines and Mark Mihalasky have been invaluable resources on GIS matters. Donald Singer has helped keep us statistically honest. For discussions about northern Great Basin geology and mineral deposits, we particularly thank David John, Ted McKee, Jim Rytuba, and Ted Theodore. The paper also benefited from excellent reviews by David B. Smith and Alan Wallace of the U.S. Geological Survey.

August 11, 2004; January 3, 2006

REFERENCES

Arehart, G.B., Chakurian, A.M., Tretbar, D.R., Christensen, J.N., McInnes, B.A., and Donelick, R.A., 2003, Evaluation of radioisotope dating of Carlin-type deposits in the Great Basin, western North America, and implications for deposit genesis: Economic Geology, v. 98, p. 235–248.

Baedecker, P.A., Grossman, J.N., and Buttleman, K.P., 1998, National geochemical data base: PLUTO geochemical data base for the United States: U.S. Geological Survey Digital Data Series report DDS-0047, 1 CD-ROM.

Blakely R.J., and Jachens, R.C., 1991, Regional study of mineral resources in Nevada—insights from three-dimensional analysis of gravity and magnetic anomalies: Geological Society of America Bulletin, v. 103, p. 795–803.

Briggs, P.H., 1996, Forty elements by inductively coupled plasma-atomic emission spectrometry: U.S. Geological Survey: U.S. Geological Survey Open-File Report 96-525, p. 77-94.

Carlson, R.W., and Hart, W.K., 1983, Geochemical study of the Steens Mountain flood basalt: Carnegie Institution of Washington Year Book, v. 82, p. 475–481.

Chaffee, M.A., 1988, Maps showing distribution of anomalies based on the use of SCORESUM plots for selected groupings of elements in samples of nonmagnetic heavy-mineral concentrate, Walker Lake 1 degrees × 2 degrees Quadrangle, California and Nevada: U.S. Geological Survey Miscellaneous Field Investigations Map MF-1382-M.

Cheng, Qiuming, 1999, Spatial and scaling modelling for geochemical anomaly separation: Journal of Geochemical Exploration, v. 65, p. 175–194.

ææ2001, Selection of multifractal scaling breaks and separation of geochemical and geophysical anomaly: Journal of China University of Geosciences, v. 12, p. 54–59.

Coombs, M.J., Kotlyar, B.B., Ludington, S., and Folger, H., 2002, Multielement geochemical dataset of surficial materials for the northern Great Basin: U.S. Geological Survey Open-file report 02-227 (URL http://geopubs.wr.usgs.gov/open-file/of02-227/).

Dunbar, N.W., Chapin, C.E., and Ennis, D.J., 1995, Arsenic enrichment during potassium metasomatism and hydrothermal processes in the Socorro, N.M. area—implications for tracing groundwater flow: New Mexico Geology, 17, 26.

Duval, J.S., 1991, Potassium, uranium and thorium geochemical maps of the conterminous United States: Transactions of Institution of Mining and Metallurgy, v. B100, p. 66–73.

Duval, J.S., and Riggle, F.E., 1999, Profiles of gamma-ray and magnetic data from aerial surveys over the conterminous United States: U. S. Geological Survey Digital Data Series Report DDS-0031, 3 CD-ROM.

Fitton, J.G., James, D., and Leeman, W.P., 1991, Basic magmatism associated with late Cenozoic extension in the western United States—compositional variations in space and time: Journal of Geophysical Research, v. 96, p. B13,693–B13,711.

Focazio, M.J., Welch, A.H., Watkins, S.A., Helsel, D.R., and Horn, M.A., 1999, A retrospective analysis on the occurrence of arsenic in ground-water resources of the United States and limitations in drinking-water-supply characterizations: U.S. Geological Survey Water-Resources Investigation Report 99-4279, 21 p.

Folger, H.W., 2000, Analytical results and sample locations of reanalyzed NURE stream-sediment and soil samples for the Humboldt River basin mineral-environmental assessment, northern Nevada: U.S. Geological Survey Open-file Report 00-421, version 1.0 (URL http://pubs.usgs.gov/open-file/of00-421/).

Glen, J.M.G., and Ponce, D.A., 2002, Large-scale fractures related to the inception of the Yellowstone hotspot: Geology, v. 30, p. 647–650.

Grauch, V.J.S., Rodriguez, B.R., and Wooden, J.L., 2003, Geophysical and isotopic constraints on crustal structure related to mineral trends in north-central Nevada and implications for tectonic history: Economic Geology, v. 98, p. 269–286.

Grosz, A.E. and Grossman, J.N., 2000, Geochemical mapping in the United States—methods, results, and implications [abs.]: International Geological Congress, 31st, Rio de Janeiro, Brazil, Aug 6–17, 2000, Abstracts, 2 p.

Gunn, B.M., and Watkins, N.D., 1970, Geochemistry of the Steens Mountain basalts, Oregon: Geological Society of America Bulletin, v. 81, p. 1497–1516.

Gustavsson, N., Bolviken, B., Smith, D.B., and Severson, R.C., 2001, Geochemical landscapes of the conterminous United States: New map presentations for 22 elements: U.S. Geological Survey Professional Paper P 1648, 38 p.

Hart, W.K., and Carlson, R.W., 1987, Tectonic controls on magma genesis and evolution in the northwestern United States: Journal of Volcanology and Geothermal Research, v. 32, p. 119–135.

Hemphill-Haley, M.A., Page, W.D., Carver, G.A., and Burke, R.M., 2000, Paleoseismicity of the Alvord fault, Steens Mountain, southeastern Oregon *in* Noller, J.S., Sowers, J.M, and Lettis, W.R., eds., Quaternary geochronology—methods and application: American Geophysical Union, Reference Shelf 4, p. 537–540.

Hess, R.H., 2001, Geothermal energy: Nevada Bureau of Mines and Geology Special Publication MI-2000, p. 43–47.

Hildenbrand, T.G., Berger, Byron, Jachens, R.C., and Ludington, Steve, 2000, Regional crustal structures and their relationship to the distribution of ore deposits in the western United States, based on magnetic and gravity data: Economic Geology, v. 95, p. 1583–1603.

Howard, K.A., 2003, Crustal structure in the Elko-Carlin region, Nevada, during Eocene gold mineralization; Ruby-East Humboldt metamorphic core complex as a guide to the deep crust: Economic Geology, v. 98, p. 249–268.

Howarth, R.J., 1983, Mapping, *in* Howarth, R.J., ed., Statistics and data analysis in geochemical prospecting: Amsterdam, Elsevier Scientific Publishing Company, Handbook of Exploration Geochemistry, v. 2, p. 111–205.

Jachens, R.C., and Moring, B.C., 1990, Maps of the thickness of Cenozoic deposits and the isostatic residual gravity over basement for Nevada: U.S. Geological Survey, Open-File Report 90–404, 15 p.

John, D.A., and Wallace, A.R., 2000, Epithermal gold-silver deposits related to the northern Nevada rift, *in* Cluer, J.K., Price, J.G., Struhsacker, E.M., Hardyman, R.F., and Morris, C.L., eds., Geology and ore deposits 2000: The Great Basin and Beyond, Geological Society of Nevada Symposium, May 15-18, Proceedings, p. 155-175.

John, D.A., Stewart, J.H., Kilburn, J.E., Silberling, N.J., and Rowan, L.C., 1993, Geology and mineral resources of the Reno 1 degree by 2 degree Quadrangle, Nevada and California: U.S. Geological Survey Bulletin 2019, 65 p.

Johnson, B.R., and Raines, G.L., 1996, Digital representation of the Idaho state geologic map: A contribution to the Interior Columbia River basin ecosystem management project: U.S. Geological Survey Open-file report 95-0690 (URL http://pubs.usgs.gov/of/1995/of95-690/).

Johnson, J.A., Hawkwsworth, C.J., Hooper, P.R., and Binger, G.B., 1998, Major- and trace-element analyses of Steens Basalt, southeastern Oregon: U.S. Geological Survey Open-File Report 98-482, 30 p.

Kilburn, J.E., Smith, D.B., and Hopkins, R.T., 1990, Analytical results and sample locality map of stream-sediment samples from the Reno 1° × 2° quadrangle, California and Nevada: U.S. Geological Survey Open-File Report 90-204, 71 p.

King, P.B., and Beikman, H.M., 1975, Geologic map of the United States (exclusive of Alaska and Hawaii): U.S. Geological Survey, scale 1:2,500,000, 3 sheets.

Kistler, R.W., 1974, Phanerozoic batholiths in western North America: A summary of some recent work on variations in time, space, chemistry, and isotopic compositions: Annual Review of Earth and Planetary Sciences, v. 2, p. 403–418.

Kistler, R.W., and Peterman, Z.E., 1973, Variations in Sr, Rb, K, Na, and initial 87Sr/86Sr in Mesozoic granitic rocks and intruded wall rocks in central California: Geological Society of America Bulletin, v. 84, p. 3489–3512.

Kotlyar, B.B., Singer, D.A., Jachens, R.C., and Theodore, T.G., 1998, Regional analysis of the distribution of gold deposits in Northeast Nevada using NURE arsenic data and geophysical data: U.S. Geological Survey Open-File Report 98-0338-B, p. 234–242.

Lindberg, D.N., 1989, Extending the zone of recognized late-Holocene faulting in the Basin and Range of southeastern Oregon [abs.]: Geological Society of America Abstracts with Programs, v. 21, p. 106.

Long, K.R., DeYoung, J.H., Jr., and Ludington, S.D., 2000, Significant deposits of gold, silver, copper, lead, and zinc in the United States: ECONOMIC GEOLOGY, v. 95, p.629–644.

Ludington, S., Cox, D.P., Leonard, K.W., and Moring, B.C., 1996a, Cenozoic volcanic geology of Nevada: Nevada Bureau of Mines and Geology Open-File Report 96-2, p.5.1–5.17 (URL http://www.nbmg.unr.edu/dox/ofr962/index.htm).

Ludington, S., McKee, E.H., Cox, D.P., Moring, B.C., and Leonard, K.W., 1996b, Pre-Tertiary geology of Nevada: Nevada Bureau of Mines and Geology Open-File Report 96-2, p.4.1-4.17 (URL http://www.nbmg.unr.edu/dox/ofr962/index.htm).

Mabey, D.R., 1965, Gravity and aeromagnetic surveys: U.S. Geological Survey Bulletin 1175, p. 105–111.

——1966, Regional gravity and magnetic anomalies in part of Eureka County, Nevada, *in* Hansen, D.A., Heinrichs, W.E., Jr., Holmer, R.C., MacDougall, R.E., Rogers, G.R., Sumner, J.S., and Ward, S.H., eds., Mining geophysics, v. 1: Tulsa, Oklahoma, Society of Exploration Geophysicists, p. 77–83.

Mankinen, E.A., Larson, E.E., Gromme, C S., Prevot, Michel, and Coe, R.S, 1987, The Steens Mountain (Oregon) geomagnetic polarity transition: 3. It's regional significance: Journal of Geophysical Research, v. 92, p. B8057–B8076.

McKee, E.H., and Blakely, R.J., 1990, Tectonic significance of linear, north-trending anomalies in north-central Nevada [abs]: Geological Society of Nevada and U.S. Geological Survey Program with Abstracts, p. 49.

McKee, E.H., Jachens, R.C., and Blakely, R.J., 1990, Major crustal differences between the northwestern part of the Great Basin and other parts of the province [abs]: Geological Society of Nevada and U.S. Geological Survey Program with Abstracts, p. 100.

Mihalasky, M.J., 2001, Mineral potential modelling of gold and silver mineralization in the Nevada Great Basin—a GIS-based analysis using weights of evidence: U.S. Geological Survey Open-File Report 01-291 (URL http://pubs.usgs.gov/of/2001/of01-291/).

Miller, R.J., Raines, G.L., and Connors, K.A., 2003, Spatial digital database for the geologic map of Oregon: U.S. Geological Survey Open file Report 03-067 (URL http://geopubs.wr.usgs.gov/open-file/of03-67/).

Motooka, J., 1996, Organometallic halide extraction for 10 elements by inductively coupled plasma-atomic emission spectrometry: U.S. Geological Survey Open-File Report 96-525, p. 102–108.

Nash, J.T., 1987, Interpretation of the regional geochemistry of the Tonopah 1 degrees by 2 degrees Quadrangle, Nevada, based on analytical results from stream-sediment and nonmagnetic heavy-mineral-concentrate samples: U.S. Geological Survey Open-File Report 87-059, 1 over-size sheet, scale 1:500,000.

Nash, J.T., and Siems, D.F., 1988, Regional geochemical maps of the Tonopah 1° × 2° quadrangle, Nevada, based on samples of stream sediment and nonmagnetic heavy-mineral concentrate: U.S. Geological Survey, Miscellaneous Field Studies Map MF-1877-B, scale 1:500,000.

Peters, S.G., 1998, Evidence for the Crescent Valley-Independence lineament, north-central Nevada: U.S. Geological Survey Open-file Report 98-0338-B, p. 106–118.

Peters, S.G., Nash, J.T., John, D.A., Spanski, G.T., King, H.D., Connors, K.A., Moring, B.C., Doebrich, J.L., McGuire, D.J., Albino, G.V., Dunn, V.C., Theodore, T.G., and Ludington, S., 1996, Metallic mineral resources in the U.S. Bureau of Land Management's Winnemucca district and Surprise resource area, northwest Nevada and northeast California: U.S. Geological Survey Open-File Report 96-0712, 146 p.

Philbin, F.W., Meuschke, J.L., and McCaslin, W.E., 1963, Aeromagnetic map of the Roberts Mountains, central Nevada: U.S. Geological Survey Open-File Report, March 7, 1963, scale 1:25,000.

Phillips, J.D., 2001, Designing matched bandpass and azimuthal filters for the separation of potential-field anomalies by source region and source type [abs]: Australian Society of Exploration Geophysicists, Geophysical Conference and Exhibition, 15th, Brisbane, Queensland, Australia, 2001, Conference Handbook ASEG 2001, CD-ROM, 4 p.

Pierce, K.L., Morgan, L.A., and Saltus, R.W., 2000. Yellowstone plume head—postulated tectonic relations to the Vancouver slab, continental boundaries, and climate: U.S. Geological Survey Open-File Report 2000-498, 29 p.

Ponce, D.A. and Glen, J.M.G., 2002, Relationship of epithermal gold deposits to large-scale fractures in northern Nevada: ECONOMIC GEOLOGY, v. 97, p. 3–9.

Raines, G.L., Connors, K.A., Moyer, L.A., and Miller, R.J., 2003, Spatial digital database for the geologic map of Nevada: U.S. Geological Survey Open File Report 03-066 (URL http://pubs.usgs.gov/of/2003/of03-66/).

Rice, K.C., 1999, Trace-element concentrations in streamed sediment across the conterminous United States: Environmental Science and Technology, v. 33, p. 2499–2504.

Roberts, R.J., 1960, Alignments of mining districts in north-central Nevada: U.S. Geological Survey Professional Paper 400-B, p. B17–B19.

Rudnick R.L. and Gao, S., 2003, Composition of the continental crust: Oxford, Elsevier, Treatise on Geochemistry, v. 3, p. 1–64.

Rytuba, J.J., Vander Meulen, D.B., and Barlock, V.E., 1991, Tectonic and stratigraphic controls on epithermal precious-metal mineralization in the northern part of the Basin and Range, Oregon, Idaho, and Nevada, *in* Buffa, R.H. and Coyner, A.R., eds., Geology and ore deposits of the Great Basin—Field Trip Guidebook Compendium, p. 636–644.

Saucedo, G.J., Bedford, D.R., Raines, G.L., Miller, R.J., and Wentworth, C.M., 2000, GIS data for the geologic map of California: California Geological Survey, CD 2000-07.

Shacklette, H.T., and Boerngen, J.G., 1984, Element concentrations in soils and other surficial materials of the conterminous United States: U.S. Geological Survey Professional Paper 574-D, 70 p.

Shevenell, L., and Garside, L.J., 2003, Nevada geothermal resources: Nevada Bureau of Mines and Geology Map 141, scale 1:1,000,000.

Smith, S.M., 2001, National geochemical databaseæreformatted data from the National Uranium Resource Evaluation (NURE) Hydrogeochemical and Stream Sediment Reconnaissance (HSSR) program, version 1.30: U.S. Geological Survey Open-File Report 97-492 (URL http://pubs.usgs.gov/of/1997/ofr-97-0492/index.html).

Stewart, J.H., and Carlson, J.E., 1978, Geologic map of Nevada: U.S. Geological Survey, scale 1:500,000.

Theodore, T.G., Kotlyar, B.B., Singer, D.A., Berger, V.I., Abbott, E.W., and Foster, A.L., 2003, Applied geochemistry, geology, and mineralogy of the northernmost Carlin trend, Nevada: ECONOMIC GEOLOGY, v. 98, p. 287–316.

Thompson, R.N., and Gibson, S.A., 1991, Subcontinental mantle plumes, hotspots, and pre-existing thinspots: Geolocial Society of London Journal, v. 148, p. 973–977.

Tingley, J.V., 1992, Mining districts of Nevada: Nevada Bureau of Mines and Geology, Report 47, 124 p.

U.S. Geological Survey, 2004, The National Geochemical Survey—database and documentation: U.S. Geological Survey, Open-File Report 2004-1001, version 1.0 (URL http://tin.er.usgs.gov/geochem/doc/home.htm).

Walker, G.W., and MacLeod, N.S., 1991, Geologic map of Oregon: U.S. Geological Survey, scale 1:500,000.

Wallace, A.R., and John, D.A., 1998, New studies of Tertiary volcanic rocks and mineral deposits, northern Nevada rift: U.S. Geological Survey Open-File Report 98-0338-B, p.

Wallace, A.R., Ludington, S., Mihalasky, M.J., Peters, S.G., Theodore, T.G., Ponce, D.A., John, D.A., and Berger, B.R., 2004, Assessment of metallic resources in the Humboldt River basin, northern Nevada: U.S. Geological Survey Bulletin 2218 (URL http://pubs.usgs.gov/bul/b2218/).

Welch, A.H., Westjohn, D.B., Helsel, D.R., and Wanty, R.B., 2000, Arsenic in ground water of the United States: Occurrence and geochemistry: Ground Water, v. 38, p. 589–604.

Xu, Yaguang, and Cheng, Qiuming, 2001, A fractal filtering technique for processing regional geochemical maps for mineral exploration: Geochemistry—Exploration, Environment, Analysis, v. 1, p. 147–156.

Zoback, M.L., and Thompson, G.A., 1978, Basin and Range rifting in northern Nevada: clues from a mid-Miocene rift and its subsequent offsets: Geology, v. 6, p. 111–116.

Zoback, M.L., McKee, E.H., Blakely, R.J., and Thompson, G.A., 1994, The northern Nevada rift: Regional tectono-magmatic relations and middle Miocene stress direction: Geological Society of America Bulletin, v. 106, p. 371–382.